micromachines

MDPI

Review

Hybrid Polymer/Metal Oxide Thin Films for High Performance, Flexible Transistors

Jae Won Jeong [1,†], Hye Suk Hwang [2,†], Dalsu Choi [3], Byung Chol Ma [4,*], Jaehan Jung [5,*] and Mincheol Chang [1,2,6,*]

1 Department of Polymer Engineering, Graduate School, Chonnam National University, Gwangju 61186, Korea; sjndow1221@naver.com
2 Alan G. MacDiarmid Energy Research Institute, Chonnam National University, Gwangju 61186, Korea; hshwang33@gmail.com
3 Department of Chemical Engineering, Myongji University, Yongin-si, Gyeonggido 17058, Korea; dalsuchoi@mju.ac.kr
4 School of Chemical Engineering, Chonnam National University, Gwangju 61186, Korea
5 Department of Materials Science and Engineering, Hongik University, Sejong 30016, Korea
6 School of Polymer Science and Engineering, Chonnam National University, Gwangju 61186, Korea
* Correspondence: anjeon@chonnam.ac.kr (B.C.M.); jaehan@hongik.ac.kr (J.J.); mchang35@chonnam.ac.kr (M.C.); Tel.: +82-62-530-1815 (B.C.M.); +82-62-530-1771 (J.J. & M.C.)
† These authors contributed equally to this work.

Received: 5 February 2020; Accepted: 3 March 2020; Published: 4 March 2020

Abstract: Metal oxides (MOs) have garnered significant attention in a variety of research fields, particularly in flexible electronics such as wearable devices, due to their superior electronic properties. Meanwhile, polymers exhibit excellent mechanical properties such as flexibility and durability, besides enabling economic solution-based fabrication. Therefore, MO/polymer nanocomposites are excellent electronic materials for use in flexible electronics owing to the confluence of the merits of their components. In this article, we review recent developments in the synthesis and fabrication techniques for MO/polymer nanocomposite-based flexible transistors. In particular, representative MO/polymer nanocomposites for flexible and transparent channel layers and gate dielectrics are introduced and their electronic properties—such as mobilities and dielectric constant—are presented. Finally, we highlight the advances in interface engineering and its influence on device electronics.

Keywords: flexible transistors; polymers; metal oxides; nanocomposites; dielectrics; active layers

1. Introduction

Thin-film transistors (TFTs) are the crucial elements in flat-panel display (FPD) applications, including both active matrix liquid crystal displays (AMLCDs) and active matrix organic light emitting diode (AMOLEDs) displays [1–3]. In recent years, the traditional amorphous Si (a-Si) TFT technology has achieved higher resolutions, larger screen sizes, and lower power consumptions in FPDs [4,5]. However, the demand for transparent, flexible, and stretchable optoelectronic devices remains, which requires further advancement in crucial component materials, including the semiconductor, the dielectric, and the conductor, as well as the substrates [6–12].

As mechanically flexible and durable semiconductors as well as gate dielectrics, metal oxides (MOs) such as In_2O_3, ZrO_2, Al_2O_3, and TiO_2 are now expected to be one of the most promising materials for next generation display technologies, because of their high carrier mobility, good transparency, excellent uniformity, and reasonable electrical reliability/stability [13–20]. More importantly, MOs exhibit high carrier mobilities even in the amorphous state and satisfactory environmental stability [21,22]. It is worth noting that the amorphous phase is favorable for use in flexible devices compared to the

crystalline phase, as crystalline materials tend to crack when folded. Indium oxide (In_2O_3) is the most heavily investigated metal oxide both as a conductor and a semiconductor, since the extensive 5s orbital overlap leads to a broad conduction band with high electron mobility even in the amorphous state [23]. Furthermore, their large bandgap ensures optical transparency. The conventional strategy to achieve optimal conductivity in In_2O_3 is to chemically dope the compound with various cations such as Sn, Ga, La, or Sc [24–26]. For example, ITO (indium−tin−oxide) exhibits excellent transparency with high conductivity since the Sn ion enhances the carrier density by donating free electrons to the lattice due to the difference in oxidation state between In^{3+} and Sn^{4+} [27,28]. In IGZO (indium−gallium−zinc−oxide), Ga forms stronger chemical bonds with oxygen and suppresses the formation of oxygen deficiencies and free electrons, thereby serving the role of a "stabilizer" or a "suppressor" [29]. Currently, commercially available metal oxide (semi)conductor films are primarily fabricated via capital-intensive vacuum vapor deposition processes, such as sputtering or thermal evaporation, thereby limiting the large scale and economic production of MO films. Post-annealing processes to enhance charge carrier mobility require high processing temperatures to induce metal–oxygen–metal lattice formation. However, such high temperatures are not suitable for fabrication of MO on soft polymeric substrates such as polyimide (PI), polyethylene naphthalate, polyethylene terephthalate, polydimethylsiloxane, and parylene [29–31]. Moreover, mechanical toughness is also required for the use of inflexible and foldable devices.

In this context, novel processing techniques for fabricating flexible MO films with high charge carrier mobilities is in great demand. Organic polymers such as poly(4-vinylphenol) (PVP), polytetrafluoroethylene (PTFE), and polyethylenimine (PEI), therefore, have been utilized as flexible matrices with various MO fillers due to their merits such as flexibility, light-weight, durability, and solution-processability [32–35]. Using MO/polymer nanocomposites, the films can be easily fabricated via solution-based fabrication processes including spin-casting and roll-to-roll.

This review seeks to summarize the recent progress in the synthesis and fabrication techniques of MO/polymer nanocomposites for flexible transistors. In particular, the synthesis of metal oxides/polymers nanocomposites for flexible channel layers and gate dielectrics, alongside their electronic properties such as mobilities and dielectric constant, are presented. Furthermore, advances in interface engineering and their influence on device electronics are highlighted.

2. Synthesis of Metal Oxides

New techniques have continued to emerge for the synthesis of MO nanostructures with controlled shape, size, and composition, because these factors play an important role in any application [36,37]. In particular, the morphology of MOs are strongly dependent on the synthetic route [38,39]. Therefore, it is critical to select an appropriate synthetic technique to achieve the desired morphology of MOs. In general, a lot of approaches have been reported for the synthesis of various MO nanostructures (Figure 1), including precipitation, hydrothermal, sol–gel methods, microwave-assisted synthesis, and chemical vapor deposition (CVD) [37,40–43].

The earliest technique that was developed to synthesize inorganics is the precipitation method. The primary merit of this strategy is its ease of scalability in the synthesis of MOs for commercialization [44]. In a typical process, the precipitation of sparingly soluble hydroxides takes place from an aqueous solution on the addition of a precipitating agent (anion) or ligand (e.g., urea, hexamethylenetetramine, and KOH) to the metal salt solution containing a cation. Subsequently, the precipitated hydroxides are decomposed to metal oxides [45]. It is very difficult to control the uniformity of the product structures via the precipitation approach, owing to a lack of understanding of major processing steps, namely nucleation and growth [46].

Hydrothermal methods are very simple and capable of generating MOs with diverse morphologies, such as spheres, rods, wires, and cones [47–50]. During synthesis, a heterogeneous reaction occurs in an aqueous solvent containing NaOH, KOH, HCl, HNO_3, H_2SO_4, etc. under a particular pressure and temperature [51]. The major benefits of hydrothermal syntheses are its low processing temperature, reduced aggregation of the products, homogeneous crystallinity of the products, and satisfactory

uniformity in composition and purity of the products [52,53]. Occasionally, surfactants such as cetyltrimethylammonium bromide, sodium dodecyl sulfate, and polyvinylpyrrolidine (PVP) are utilized—the surfactant molecules selectively adhere onto the polar surface of the MO crystals, controlling the shape and growth behavior of MO particles [54–56].

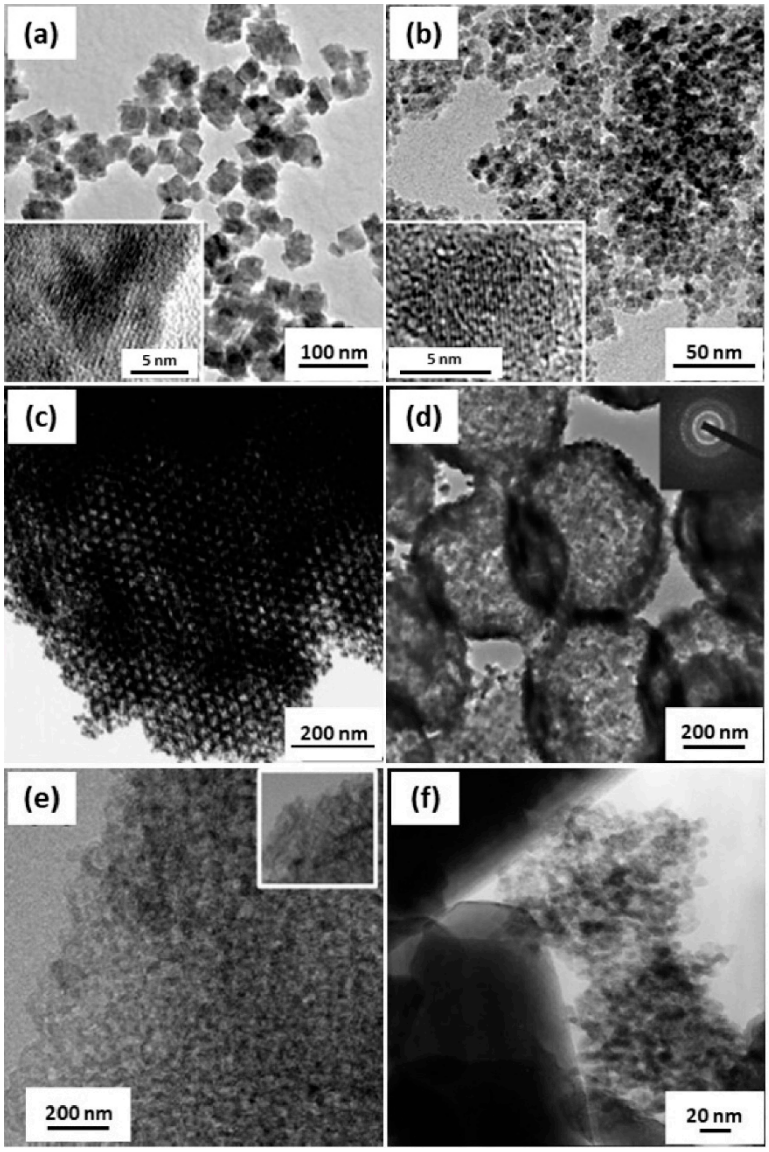

Figure 1. (**a**–**f**) A set of TEM images of diverse MO nanostructures: (**a**) MnO and (**b**) Fe_3O_4 nanoparticles fabricated via microwave-assisted synthesis (Reproduced from [42], Copyright 2008 Royal Society of Chemistry C), (**c**) porous SnO_2 aerosols prepared via sol–gel method (reproduced with permission from [41], Copyright 2005 Wiley-VCH Verlag GmbH & Co. KGaA, Weinheim), (**d**) ZnO hollow spheres synthesized via hydrothermal synthesis (reproduced with permission from [40], Copyright 2008 American Chemical Society), (**e**) In_2O_3 nanoparticles prepared via anodization-precipitation (reproduced with permission from [37], Copyright 2018 American Chemical Society), and (**f**) TiO_2 nanoparticle layer on SiO_2 prepared via CVD, respectively (reproduced with permission from [43], Copyright 2001 Elsevier).

Sol–gel is a general, versatile, and powerful approach for the synthesis of single- or multiple-component MO nanostructures in the form of thin films, powders, and porous materials. This approach is a cost effective and low-temperature process that enables the production of MO

nanostructures with high homogeneity and compositional purity [57,58]. Metal alkoxides [$M(OR)_3$] are primarily used as a precursor to prepare MOs due to their propensity to form homogeneous solution in a variety of solvents in the presence of other alkoxides or metallic derivatives and also due to their reactivity toward nucleophiles such as water [59]. The sol–gel process involves several important steps, such as hydrolysis and condensation, gelation, and drying (Figure 2). Typically, metal precursors such as metal alkoxides and metal chlorides undergo the reactions of hydrolysis and partial condensation to form a colloidal solution. Subsequently, three-dimensional gels are formed immediately via polycondensation of the hydrolyzed precursors. Finally, the resultant gels are converted to xerogel or aerogel based on the method of drying (i.e., supercritical drying or ambient drying) and, furthermore, to the desired MO materials via a thermal treatment. The sol–gel technique can be divided into two routes—namely the aqueous sol–gel and the nonaqueous sol–gel methods. The aqueous sol–gel method requires oxygen for the formation of MOs, which is generally provided by the water solvent. However, this approach is not suitable for the production of MO nanomaterials because the crucial steps (i.e., hydrolysis, condensation, and drying) take place simultaneously and thus result in the formation of bulk MOs [39,60]. In contrast, solvents such as alcohols, ketones, and aldehydes are used to provide the oxygen necessary for the formation of MOs via the nonaqueous sol–gel method [39,61–63]. Additionally, this approach is suitable for the production of MO nanomaterials, rather than their bulk counterparts. The organic solvents serve as important components by controlling morphology, particle size, surface properties, and composition of the resultant MO materials [64].

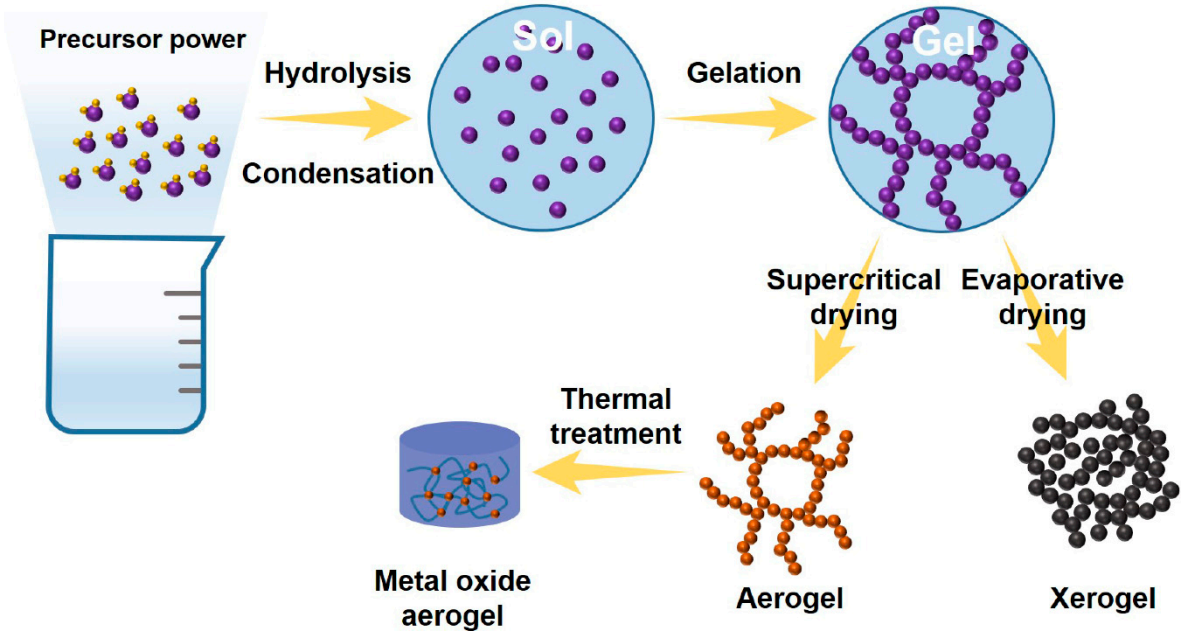

Figure 2. Reaction routes for the production of MO nanostructures by the sol–gel method.

Microwave-assisted synthesis is an approach that applies microwave radiation to chemical reactions for the production of MO nanostructures. This method could allow more efficient, rapid, and homogenous heating of reaction mixtures, thereby accelerating the synthesis of MO nanostructures [65]. Furthermore, the formation of fine MO nanocrystals is enabled by the use of microwave radiation due to the highly focused local heating that can be achieved [66]. Moreover, the microwave-assisted approach can produce a wide range of MO nanostructures, including nanoflakes [67], nanosheets [68], and nanoflowers [69]. However, the microwave-assisted synthesis possesses some drawbacks, such as the high cost of microwave reactor and the limited penetration depth of microwave radiation, indicative of restricted scalability for the commercial synthesis of MO nanoparticles [70].

3. Metal Oxide/Polymer Hybrid Films in Transistors

3.1. Active Channel Layers

Although metal oxides (MOs) exhibit high carrier mobilities and good environmental stability even in the amorphous state, their application in flexible and stretchable devices has been rather limited [25,71–73]. This is because polycrystalline materials suffer from crack formation at the grain boundaries leading to drastic deterioration of structural integrity [74–78]. Recently, amorphous metal oxides (MOs) have been prepared to improve flexibility. However, they are still vulnerable to mechanical stress, yielding cracks under repeated mechanical deformation. On the other hand, polymers exhibit flexibility, solution-processability, and excellent compatibility with organic substrates or active layers [79,80]. In this context, organic–inorganic nanocomposites can gain the synergetic advantages of these two components—namely, mechanical toughness, flexibility, and high mobility [81,82]. Moreover, the incorporation of polymers with MOs successfully inhibits the formation of the crystalline phase which is detrimental to flexible substrates. It should be noted that in general, the trade-off between the mechanical properties and electrical properties is observed in MO/polymer nanocomposites. In other words, while incorporation of polymers to MO films gives rise to an increase in flexibility, it leads to a potential reduction in electrical properties due to phase separations and lack of interconnectivity of MO domains in the resultant composite films. To overcome the issue, various strategies that can improve the interconnectivity of MO domains within the composite films have emerged in recent years, including engineering of weight fraction, surface modification, and morphology control of MO nanoparticles [83–86].

To improve mechanical flexibility of metal oxide (MO) films, polymers such as poly(4-vinylphenol) (PVP), polytetrafluoroethylene (PTFE), and polyethylenimine (PEI) were utilized as doping agents to improve flexibility, as well as to form the amorphous phase of MO [35,87–90]. For example, Yu et al. developed a new low temperature approach to high-mobility amorphous metal oxide semiconductor films via doping with an insulating polymer, poly(4-vinylphenol) (PVP), to fabricate amorphous MO: polymer blend composites, as depicted in Figure 3a [91]. It should be noted that PVP possesses excellent solubility in the In_2O_3 precursor solution and their hydroxyl groups favor coordination with the MO lattice. Such an approach effectively prevents crystallization, controls the carrier concentration in the In_2O_3 channel, and retains conducting pathways for efficient charge transportation. In greater detail, all-amorphous and transparent bottom-gate top-contact thin-film transistors (TFTs) were fabricated via spin-coating of In_2O/PVP precursor solutions on AryLite substrates and annealing at 225–250 °C. They exhibited high transparency (< 80%) and low sheet resistance (< F Ω sq^{-1}). In_2O_3: 5% PVP TFTs exhibited electron mobilities of 11 cm^2 V^{-1} s^{-1}. As the amount of PVP content increases, the In_2O_3 films become amorphous even with 1 wt % of PVP, as confirmed by grazing incidence X-ray diffraction (GIXRD)(Figure 3b). V_T shifts to a positive value and the mobility slightly decreases upon incorporation of PVP, as evidenced in Figure 3c, owing to the carrier concentration modulation from PVP-induced electron traps. The bending/relaxation measurement is to characterize durability of flexible films. A film is bended and relaxed several times with defined radius and then electronic properties are measured. It is worth noting that smaller radius is for more harsh condition; the bending radii that are required for flexible, rollable, and foldable displays are 0r, 10r, and 1r, respectively [92]. The bending tests indicate that the In_2O_3: 5%PVP hybrid films exhibit only a slight decrease in the mobility from 10.9 to 8.9 cm^2 V^{-1} s^{-1} as the bending radius decreases to 10 mm, while the pristine In_2O_3 films, in stark contrast, show dramatic deterioration of the mobility from 22.2 to 0.5 cm^2 V^{-1} s^{-1} (Figure 3d). Importantly, the value retains up to ca. 90% of their performance even after undergoing repeated mechanical stress (bending/relaxing 100 times).

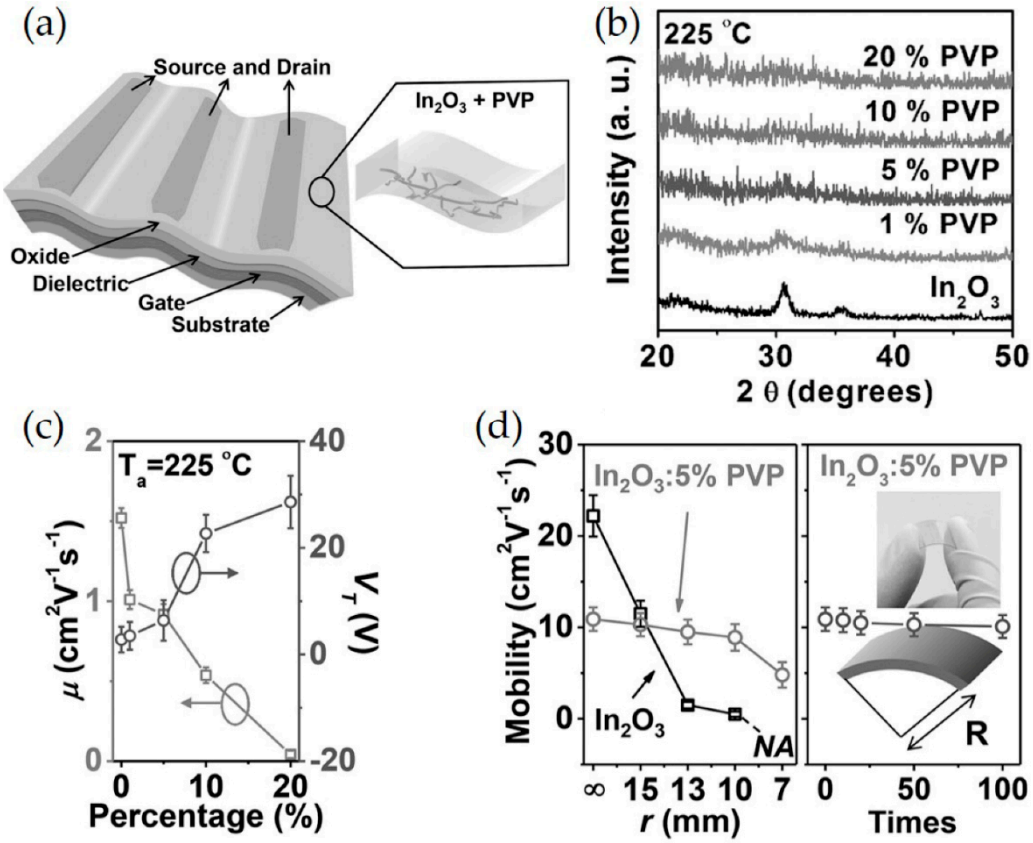

Figure 3. (**a**) Schematic representation of the flexible, transparent TFT structure based on a metal oxide:polymer (In_2O_3: *x*% PVP) semiconductor blend. (**b**) X-ray diffraction (XRD) patterns of In_2O_3: polymer films with various PVP concentrations: annealing at 225 °C. (**c**) TFT mobility and threshold voltage for In_2O_3: polymer films having different PVP concentrations, processed at 225 °C. (**d**) Dependence of TFT mobilities on bending radius of both neat In_2O_3 TFTs and all-amorphous In_2O_3: 5% PVP TFTs (left), and mobilities on all-amorphous TFT bending cycles at a radius of 10 mm. Inset: Optical image of transparent flexible TFTs. Reproduced with permission from [91], Copyright 2015 Wiley-VCH Verlag GmbH & Co. KGaA, Weinheim.

Polyethylenimine (PEI) is a commercially available polymer capable of efficient n-doping due to the electron-donating nature of the tertiary amine groups (Figure 4a). PEI electron doping has been reported for several organic semiconductors and is widely used in organic photovoltaic cells and transistors to enhance the charge transportation in other organic materials. In this context, Huang et al. fabricated In_2O_3 / PEI TFT devices via doping of metal oxides with PEI [93]. Doping of In_2O_3 with PEI effectively prevents crystallization of MOs, controls the carrier concentration in the In_2O_3 channel, and increases the electron mobility of the In_2O_3 matrix. In greater detail, a PEI-doped In_2O_3 blend (i.e., aqueous PEI-In_2O_3 precursor solutions) was coated on Si substrates with 300 nm SiO_2, followed by annealing at 250 °C for 30 min. The addition of PEI successfully inhibits the formation of crystalline structure, which is unfavorable for application in flexible devices as characterized by GIXRD in Figure 4b. The characteristic peaks at 22.1°, 31.1°, 36.0°, and 46.3° ascribed to crystalline In_2O_3 are strongly suppressed even with a PEI concentration of >1%. Extended X-ray absorption fine structure (EXAFS) measurements correlate the effect of PEI with the TFT mobility. The coordination number (CN) of In-O at the first shell remains intact independent of the PEI doping concentrations, while the second shell CN exhibits the PEI content dependency, decreasing from 6 to 4.05 as the PEI concentration increases (Figure 4c). This indicates that PEI disrupts the formation of lattices, and thus electron conduction pathways. The devices fabricated with polymer concentration of 1–1.5% resulted

in excellent mobility up to 9 cm^2 V^{-1} s^{-1} and high on/off ratio of 10^7, while that fabricated with pure In_2O_3 only exhibited a maximum value of 9 cm^2 V^{-1} s^{-1} (Figure 4d). It is because the electron donating nature of PEI results in doping of In_2O_3 and matrix film microstructure tuning, yielding high mobilities alongside optimal off-current (I_{off}) and threshold voltage (V_{th}).

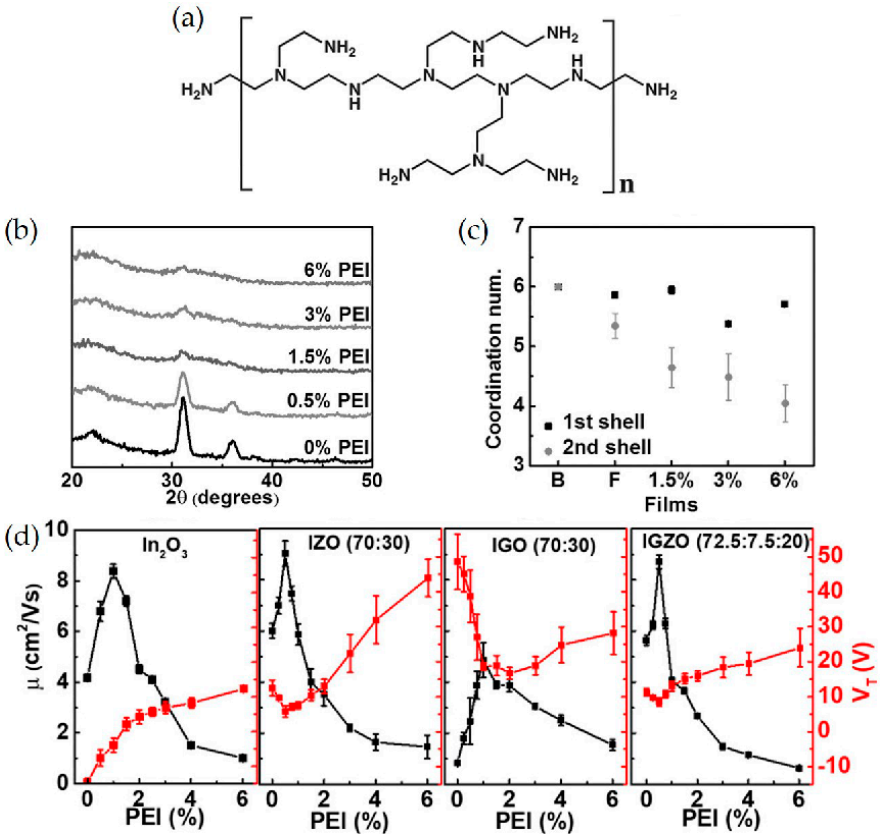

Figure 4. (**a**) Chemical structure of PEI. (**b**) GIXRD patterns of In_2O_3: x% PEI blend films with differing PEI concentrations. (**c**) Derived coordination number, In-O bond lengths for the indicated films. (**d**) TFT mobility and threshold voltage for In_2O_3: *x* wt % PEI (250 °C), IZO: *x* wt % PEI, IGO: *x* wt % PEI, and IGZO: *x* wt % PEI, as a function of the polymer concentration. $T_{annealing}$ = 300 °C. Reproduced with permission from [93], Copyright, 2016 Wiley-VCH Verlag GmbH & Co. KGaA, Weinheim.

The same research group also investigated the charge transportation and film microstructure evolution of PEI-doped amorphous Zn- and/or Ga-incorporated In_2O_3 thin films [94]. PEI doping generality was expanded from binary In_2O_3 to ternary (e.g., In + Zn in IZO, In + Ga in IGO) and quaternary (e.g., In + Zn + Ga in IGZO) metal oxide matrices. PEI-metal oxide precursor solutions on Si wafers with 300 nm wide thermally grown SiO_2 layers were first spin-casted and then thermally annealed at 300 °C. In this study, the effect of PEI doping concentration and the addition of secondary ions (Ga and Zn) to In_2O_3 on the device performance was investigated. It was found that the incorporation of Zn and PEI in In_2O_3 and IGO led to an increase in the surface roughness, thereby degrading the charge transport properties. The crystallinity of In_2O_3 or IG(Z)O was effectively suppressed and it was observed to monotonically decrease as the PEI concentration was increased. The layer formed adjacent to the dielectric improves the efficiency of charge transportation in a channel when PEI content is low because of trap prefilling. When PEI concentration exceeds a certain threshold, the mobility of the resulting devices begins to decrease due to the disruptions in film continuity and increased trap sites.

Na et al. demonstrated flexible IGZO:PTFE TFTs with improved stability and endurability against water exposure using the facile method of blending the MO semiconductor with polytetrafluoroethylene

(PTFE) via plasma polymerization [95]. In greater detail, the IGZO: PTFE layer was co-sputtered with radio frequency magnetron sputtering processes. The hydrophobic nature of PTFE enhances device performance (μ_{FE} exceeding 10 cm^2 V^{-1} s^{-1}) and stability (a V_{th} shift of 0.68 V after an hour of immersion in water) by preventing the adsorption of water molecules on the back surface of TFTs (Figure 5a). Such an approach also improves the electrical stability of IGZO: PTFE TFTs in positive bias stress (PBS), positive bias temperature stress (PBTS), positive bias illumination stress (PBIS), negative bias stress (NBS), negative bias temperature stress (NBTS), and negative bias illumination stress (NBIS) stability tests. Indeed, V_{th} of IGZO: PTFE TFT remains steady, with only a shift of 0.68 V, while that of IGZO TFTs exhibits significant negative shifts by 12.17 V, as depicted in Figure 5b,c. The improved mechanical flexibility resulting from the soft nature of PTFE enhances the mechanical durability, as depicted in Figure 5d. Specifically, the IGZO: PTFE TFT can retain its performance with no substantial change in its electrical characteristics (a V_{th} shift of 0.89 V from 3.95 to 3.06 V) over 10000 bending cycles with a bending radius of 5 mm. In contrast, the IGZO TFTs exhibit a significant V_{th} shift of 5.45 V, from 3.07 to −2.38 V.

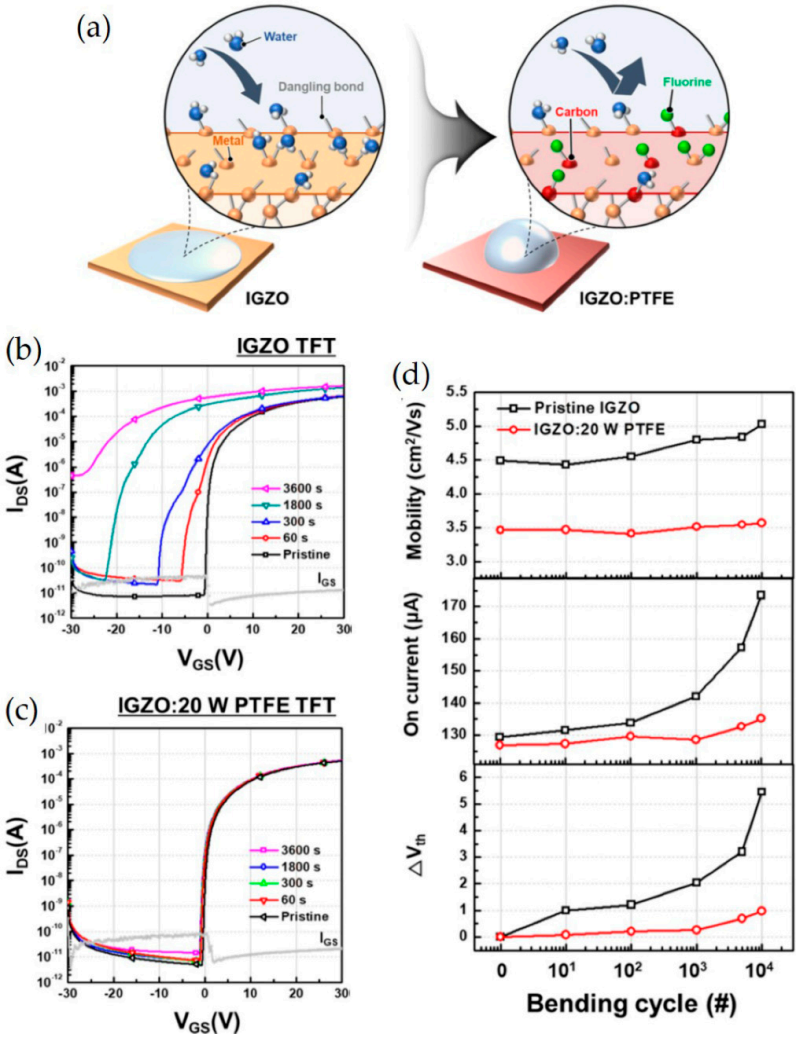

Figure 5. (**a**) Schematic illustration of improved hydrophobicity of the IGZO: PTFE film. Transfer characteristics of (**b**) the IGZO TFT and (**c**) the IGZO: 20 W PTFE TFT upon exposure to water for different times. (**d**) Variations of mobility (μ_{FE}), on-current, and V_{th} for IGZO and IGZO: 20 W PTFE TFTs with respect to bending cycles. Reproduced permission from [95], Copyright, 2018, American Chemical Society.

Sun et al. reported a strategy to control the geometry and enhance device performance of inkjet-printed MOTFT arrays via the addition of an insulating polymer to the precursor solution prior to film deposition [96]. To prevent the formation of a non-uniform geometry during inkjet-printing, the polymer additive, polystyrene (PS) was utilized. It was reported that the addition of high viscous polymers is favorable to eliminate coffee ring effects by significantly reducing the solute mobility and thus suppressing outward capillary flow of solute to the edge. In detail, PS, with different molecular weights ranging from 2000 to 2,000,000, was mixed with indium precursors (i.e., indium nitrate hydrate) and then printed on silicon substrates, followed by annealing at 225 °C for 1 h. Interestingly, 202 with an increase in PS MW, the coffee ring effect gradually faded, as measured by optical microscope in Figure 6a. The change in surface morphology by varying PS MW is attributed to the suppressed capillary flow and the Marangoni effect. The relative viscosities of In_2O_3/PS precursor solutions to those of pristine In_2O_3 solution are 1.02, 1.17, 1.39, and 1.31 for PS with MW of 2000, 20,000, 200,000, and 2,000,000, respectively. Evidently, the use of PS with MW of 20,000 results in smooth films as the increased viscosity inhibits the capillary flow, thus facilitating the depinning of the contact line. The incorporation of PS results in the improvement of carrier mobility from 4.2 cm^2 V^{-1} s^{-1} up to 13.7 cm^2 V^{-1} s^{-1} as PS MW increases from 2000 to 2,000,000, which is about three times that of the pristine In_2O_3 TFTs (Figure 6b). The trap densities for pristine, PS Mw of 2000, 20,000, 200,000, and 2,000,000 were 2.4×10^{12}, 1.2×10^{12}, 1.1×10^{12}, 1.0×10^{12}, and 1.1×10^{12} cm^{-2} eV^{-1}, respectively. XPS characterization shows that the incorporation of PS obviously impacts local bonding of MO:PS blends, thereby increasing M-O concentration (Figure 6c). Grazing incidence X-ray diffraction indicates that the addition of PS favors the formation of amorphous phase and enhances the M-O lattice contents, both of which facilitate the carrier transportation.

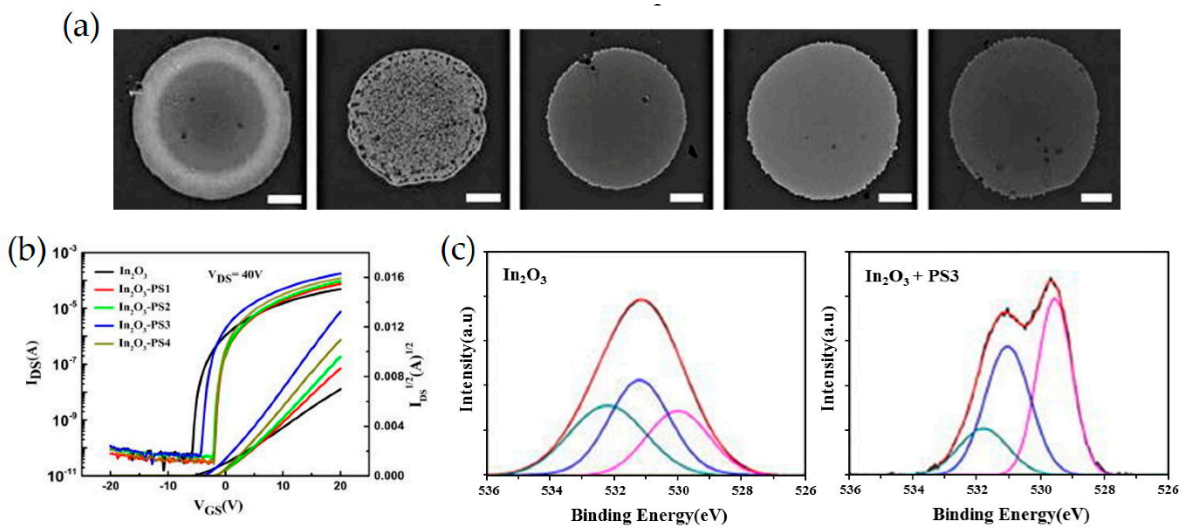

Figure 6. (**a**) Optical microscopy images of In_2O_3 deposition (right to left) without PS, with PS1, with PS2, with PS3, and with PS4. The scale bar is 100 μm. (**b**) Transfer characteristics of inkjet-printed TFTs. (**c**) X-ray photoelectron spectroscopy (XPS) of O 1s spectra. Reproduced with permission from [96], Copyright 2018, American Institute of Physics.

3.2. Dielectric Layers

MOs have been considered to be a crucial component in thin-film electronic systems due to their outstanding electrical and mechanical properties [97–104]. However, the MOs lack flexibility, which limits their use in flexible electronics [105]. Thus far, most thin high-k inorganic metal oxide dielectrics have been fabricated via conventional vacuum-based techniques including pulsed laser deposition (PLD), atomic layer deposition (ALD), magnetron sputtering, and e-beam evaporation. However, these methods are costly and unsuitable to produce large-area flexible oxide electronics. For example, high-quality gate dielectric SiO_2 films are produced via expensive vacuum-based

plasma-enhanced chemical vapor deposition (PECVD) at high temperatures above 300 °C. It is worth noting that such high temperatures may cause deformation or warping of flexible substrates. Although high performances have been achieved, flexibility and stability still limit their application in real products such as wearable devices. Moreover, dielectric layers (e.g., SiO_2) are vulnerable to mechanical stress notwithstanding their extremely thin width, yielding cracks or delamination under mechanical deformation even at small bending radii. In this context, organic dielectrics have garnered substantial attention in the area of flexible devices owing to their flexibility, mechanical stability, low temperature, easy solution processability, and excellent compatibility with flexible organic substrates, despite their low k value [105–110]. Therefore, hybridization of organic and inorganic materials can lead to the improvement in flexibility, dielectric constant, and mechanical toughness of gate dielectric materials [111–119]. The transistor parameters critically depend on the interface formed between dielectric and semiconductor layers since the trapped charges strongly impact the electrical behavior. The hybrid gate dielectrics tend to be compatible with either organic or inorganic semiconductors. As the inorganic constituent, high-k inorganic nanoparticles such as ZrO_2, Al_2O_3, Y_2O_3, Ta_2O_5, and TiO_2 were usually embedded in a polymeric matrix such as poly(methylmethacrylate) (PMMA) and poly(vinylpyrrolidone) [120–122]. However, the inorganic nanoparticles tend to agglomerate, increasing the surface roughness of the hybrid layers, resulting in high gate leakage current and low on/off current ratio. In this section, the development of hybrid organic–inorganic composites with low power consumption, low operating voltage, and compatibility with transparent flexible electronics for the use in dielectric layers will be summarized.

Poly(methyl methacrylate) (PMMA) is an important thermoplastic polymer with excellent transparency, a refractive index of n = 1.49, good chemical resistance, thermal stability, mechanical flexibility, low cost, and a lower dielectric constant (2.9) than that of silicon oxide material (3.9) [123–126]. As a result, PMMA has been mixed with high-k inorganic nanoparticles such as ZrO_2, Al_2O_3, and TiO_2 to provide high optical transparency, low weight, mechanical flexibility, and formability [14,127,128]. The low temperature deposition process towards PMMA-ZrO_2 nanocomposites as dielectric gate layers has been reported [129]. Intriguingly, to prevent phase separation, inorganic oxides were cross-linked with PMMA and trimethoxy-silyl-propyl-methacrylate (TMSPM) molecules that are chemically compatible with both inorganic and organic phases. In greater detail, TFT devices with a ZnO/PMMA-ZrO_2/ITO/glass structure (Figure 7a) were fabricated and their electrical properties, such as threshold voltage, channel mobility, and I_{on}/I_{off} current ratio, were investigated. A hybrid dielectric layer was prepared via a sol−gel reaction among zirconium propoxide (ZP), TMSPM, and methylmethacrylate (MMA) precursors at variable TMSPM molar ratios. The devices fabricated with 0.3 M TMSPM exhibit a mobility of 0.48 cm^2/V s, on/off ratio of 10^6–10^7, and a threshold voltage of 3.3 V. The leakage current density increases from 10^{-6} to 10^{-5} A/cm^2 as the amount of TMSPM content increases in the hybrid insulating layer, as illustrated in the current density versus electric field characteristic curves (Figure 7b). Importantly, the threshold voltage of the devices decreases from 3.3 V to 0.9 V with an increase in the TMSPM amount from 0.3 M to 0.75 M, as measured by transfer curves in Figure 7c. This feature is advantageous for low power consumption.

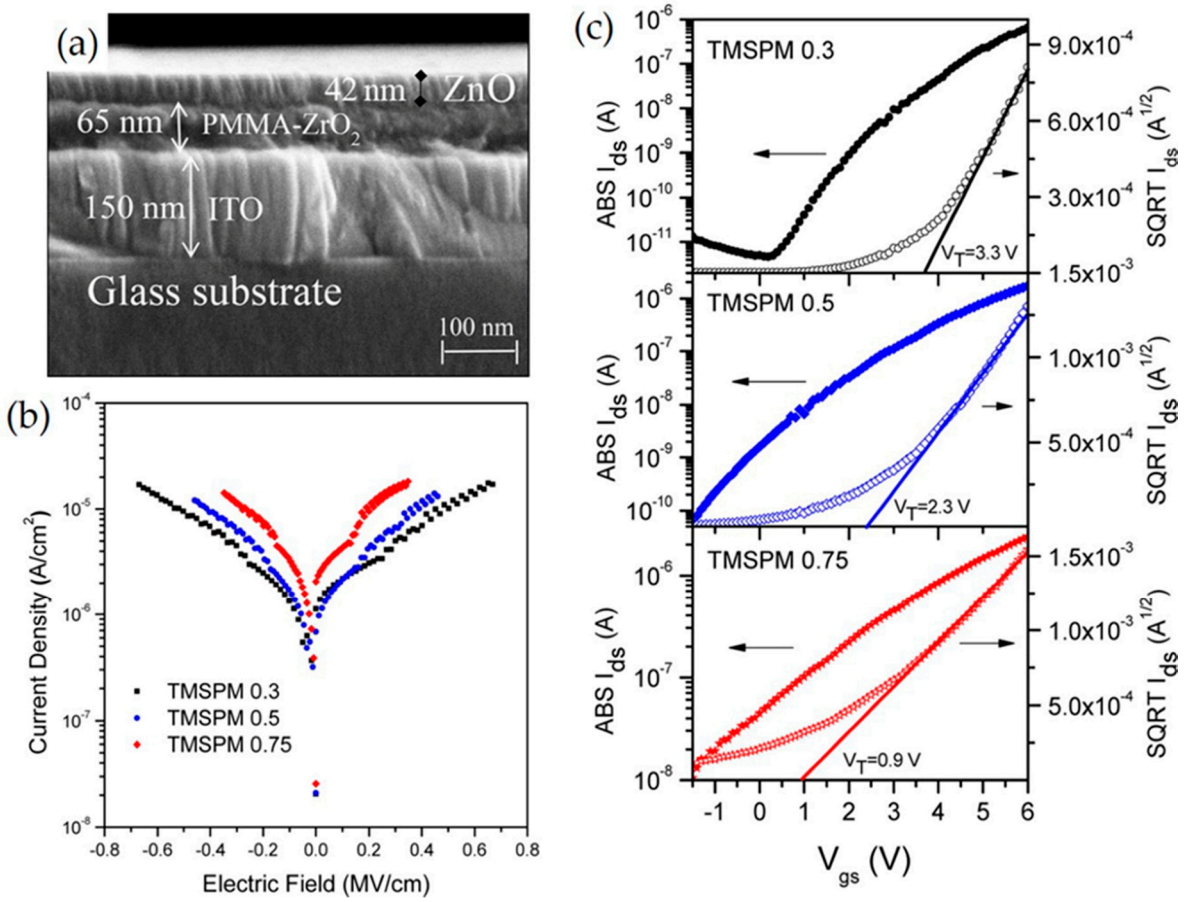

Figure 7. (**a**) SEM image of the TFT cross section, where the PMMA–ZrO_2 layer was deposited with 1:0.3:1 molar ratio. (**b**) Leakage current density vs. electric field of the PMMA–ZrO_2 hybrid layers deposited with different TMSPM molar ratios. (**c**) Transfer characteristics for ZnO-based transistors with PMMA–ZrO_2 as gate dielectric hybrid films at different TMSPM molar concentrations. Reproduced with permission from [126], Copyright 2017, American Chemical Society.

Yttrium oxide (Y_2O_3) nanoparticles exhibit a wide band gap of 6.0 eV, which is advantageous to the aspects of illumination stability of TFTs [130]. In this context, TFTs were fabricated on polyimide (PI) substrates using cross-linked poly(4-vinylphenol) (c-PVP)/ Y_2O_3 nanocomposites as gate insulators [131]. The architecture of the flexible devices was Ag/6,13-bis(triisopropylsilylehtynyl)pentacene(TIPS-pentacene)/ c-PVP:Y_2O_3/c-PVP/PI. In greater detail, the cross-linkable PVP was prepared by dissolving PVP and a cross-linking agent, (methylated poly(melamine-co-formaldehyde), MMF) in propylene glycol methyl ether acetate (PGMEA). TFTs with c-PVP:Y_2O_3 hybrid dielectric exhibited an on-state drain current of −0.165 μA at a gate voltage of −40 V, which is higher than that of devices with only c-PVP (−0.0462 μA), as depicted in Figure 8a,b. However, as illustrated in Figure 8c,d the c-PVP/Y_2O_3 composite films exhibited a higher roughness compared to the c-PVP films, leading to a larger interference in hole conduction at the interface between the insulator and the semiconductor. Additionally, c-PVP: Y_2O_3-based TFTs exhibited a greater number of leakage paths for the gate current compared to c-PVP-based TFTs, possibly owing to several interactions like i) the attraction of hole carriers by the highly polarized Y_2O_3 nanoparticles, ii) flow along the direction of the gate electric field, and iii) repulsion by the positive side and attraction by other adjacent side of the Y_2O_3 nanoparticles (Figure 8e–g).

Kim et al. have introduced TiO_2-polymer composites via cross-linking reactions of these two constituents with low surface energy which allows vertical growth of organic molecules (e.g., pentacene) [132]. In greater detail, a TiO_2 precursor (titanium(IV) butoxide and acetyl acetone)

and poly(4-vinylphenol) (PVP) solution (PVP, poly(melamine-co-formaldehyde) methylated/butylated and propylene glycol methyl ether acetate (PGMEA) solvent) mixture were spin-coated on ITO substrates and then annealed at 200 °C for 1 h. Interestingly, poly(melamine-co-formaldehyde) methylated/butylated acts as the cross-linker, which reacts with the hydroxyl group of the PVP and the ligands of the TiO_2, forming a dense structure. The resulting device exhibits a charge carrier mobility of 0.105 cm^2 V^{-1} s^{-1}, on/off ratio of 10^3, and a leakage current of 10^{-7} A cm^{-2} at ±5 V due to such a dense structure. Furthermore, this homogeneous TiO_2-polymer composite solution is stable in ambient conditions. Bang et al. fabricated bottom-gate ZnO-thin film transistors using PVP/Al_2O_3 dielectrics and investigated the effects of an organic/inorganic dielectric on device performance [133]. The leakage current of the PVP/Al_2O_3 dielectric improved by three times over the PVP counterparts. The saturation mobility of PVP/Al_2O_3 TFTs also improved from 0.05 to 0.8 cm^2 V^{-1} s^{-1} compared to PVP TFTs.

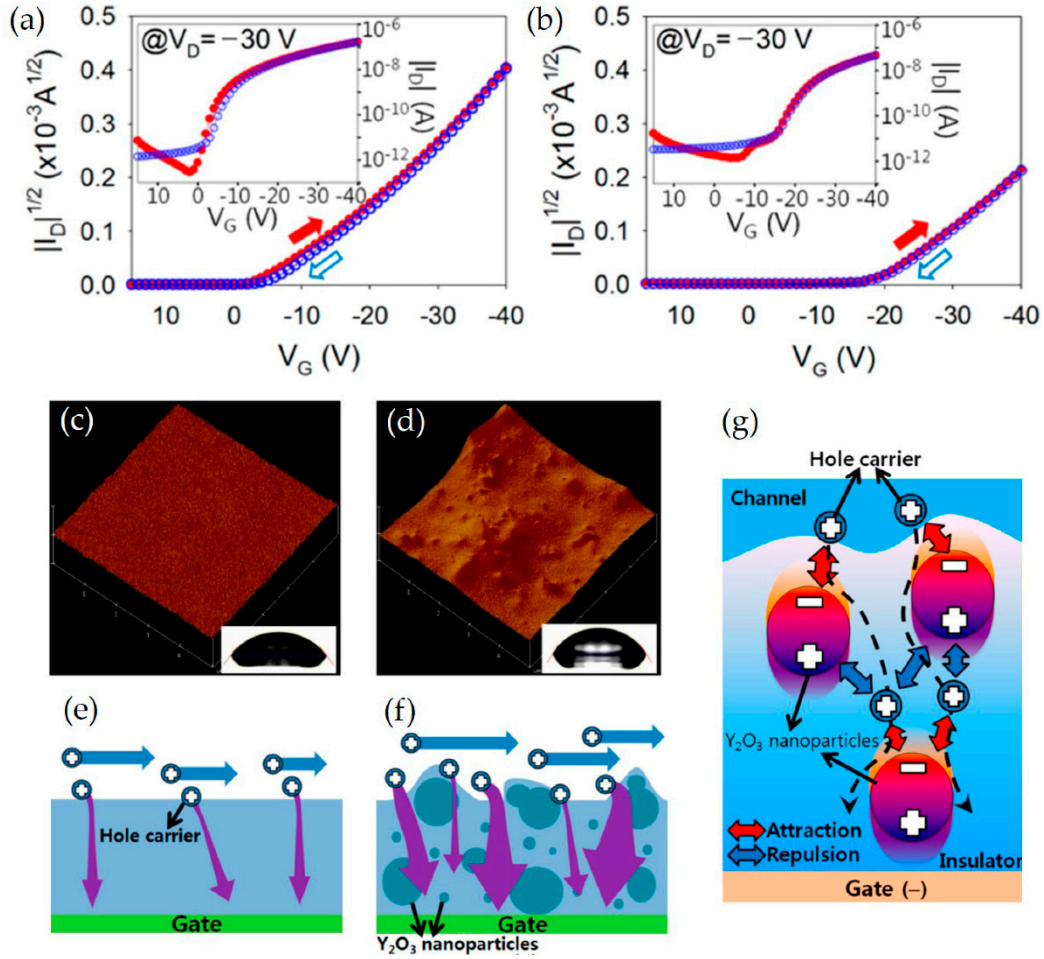

Figure 8. $|I_D|^{1/2}$ vs. V_G plots of TIPS-pentacene TFTs with the (**a**) c-PVP/Y_2O_3 composite and (**b**) c-PVP gate insulators. AFM images of the (**c**) c-PVP and (**d**) c-PVP/Y_2O_3composite films. The insets show the contact angles on both films. Leakage current paths through the (**e**) c-PVP/Y_2O_3 composite and (**f**) c-PVP gate insulators. (**g**) Possible interaction between the holes and the Y_2O_3 nanoparticles in the c-PVP/Y_2O_3 composite insulator. Reproduced with permission from [131], Copyright 2016, MDPI, Basel, Switzerland.

Despite superior mechanical flexibility, organic materials as gate insulators, such as poly-4-vinylphenol (PVP) and polymethyl methacrylate (PMMA), exhibit very low capacitance compared to inorganic dielectrics. In this context, several approaches to improve the capacitance have been introduced. This includes reducing the thickness of dielectric films and incorporating high-k inorganic nanoparticles. However, the use of ultra-thin organic dielectrics often resulted

in structural imperfections, producing current leakage. Kim et al. proposed a novel vapor-phase synthesis method to form an ultrathin, homogeneous, high-k organic–inorganic hybrid dielectric [134]. Hybrid dielectrics are synthesized via initiated chemical vapor deposition (iCVD) in a one-step manner (Figure 9a). This method utilizes 2-hydroxyethyl methacrylate and trimethylaluminum as the monomer and the inorganic precursor, respectively. A uniform and defect-free hybrid dielectric layer with precise thickness below 20 nm and composition can be produced. The hybrid films are formed via following subsequent steps—the injection of vaporized monomers, precursors, and initiators, the thermal decomposition of initiators to form free radicals, the adsorption of monomers and precursors, and free-radical polymerization of monomers. The hybrid dielectric exhibits a high k-value of 7 and a low leakage current density of less than 3×10^{-7} A/cm^2 at 2 MV/cm, even with a thickness of less than 5 nm. The capacitance (C_i) versus electric field and the current density (J) versus electric field characterizations corresponding to varying hybrid film thicknesses were also investigated, as illustrated in Figure 9b. As the thickness decreases, the C_i and J values reach 250 nF/cm^2 and 1×10^{-7} A/cm^2, respectively. The n- and p-type OTFTs were fabricated using the hybrid dielectric deposited via the iCVD process and their charge-transfer curves were studied, as depicted in Figure 9c,d. The hybrid dielectric offered a superior interface between the channel and dielectric and thus induced ideal charge-transfer characteristics. Both n- and p-type OFETs with the hybrid dielectric exhibited no apparent hysteresis and a low leakage current density (<3×10^{-7}A/cm^2 at 2 MV/cm). Furthermore, the dielectric layer exhibited improved chemical stability without any degradation in its dielectric performance. Interestingly, the hybrid dielectric layer retained its excellent dielectric performance under tensile strains of up to 2.6%.

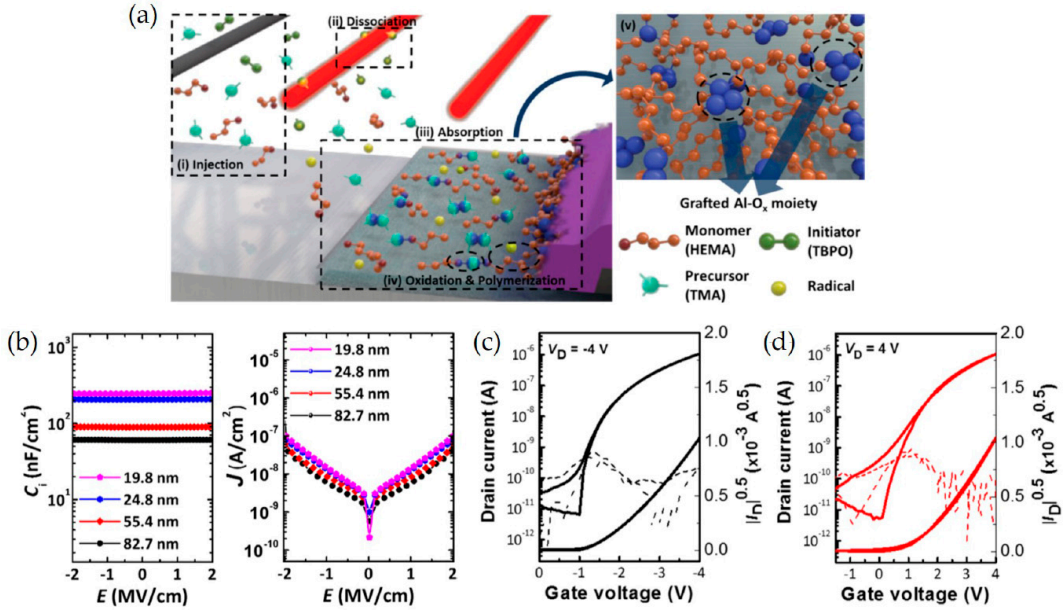

Figure 9. Vapor-phase synthesis of organic–inorganic hybrid dielectrics via iCVD. (**a**) A schematic of the synthesis process: (**i**) Vaporized monomers, organometallic precursor, and initiators are injected. (**ii**) The initiators were thermally decomposed near the heated filament to form radicals (red lines), which are positioned away from the substrate. (**iii**) Monomers, precursor, and radicals were absorbed on the heated substrate. (**iv**) The adsorbed monomers were polymerized and simultaneously reacted with inorganic precursors. (**v**) Uniform dispersion of the inorganic oxides can be achieved in the polymer matrix. (**b**) C_i–E(left), and J–E(right) characteristics of the MIM devices with the hybrid dielectrics (Al concentration: 17.8%) with various thicknesses of 82.7, 55.4, 24.8, and 19.8 nm, respectively. Charge-transfer characteristics of the (**c**) pentacene and (**d**) PTCDI-C13 OTFTs, respectively. Hybrid films 25 and 34 nm thick were used as the gate dielectric for pentacene and PTCDI-C13 OTFTs, respectively. Reproduced with permission from [134], Copyright 2018, American Chemical Society.

The effects of the device architecture on indium zinc oxide (IZO) TFTs with poly(4-vinylphenol-co-methylmethacrylate) (PVP-co-PMMA) gate insulators were investigated [135]. The top gate IZO TFTs exhibited the improved μ_{FE}, SS, V_{th}, and good Ion/off ratio of 8.5 cm^2 V^{-1} s^{-1}, 2.0 V per decade, -10.0 V, and 10^7, respectively, compared to the bottom gate IZO TFTs (μ_{FE}, SS, V_{th}, and Ion/off ratio were 9.0 cm^2 V^{-1} s^{-1}, 5.0 V per decade, −12.5 V, and 2×10^5, respectively). This is attributed to the energetic ion bombardment in the polymer gate dielectric layer during the sputtering process. The device performance can be further improved by doping the hybrid PVP-co-PMMA gate dielectric with ZrO_2: the μ_{FE}, SS, V_{th} and $I_{on/off}$ ratio in this case were 28.4 cm^2 V^{-1} s^{-1}, 0.70 V per decade, −2.0, and 4.0×10^7, respectively.

To improve surface contact with organic molecules and increase dielectric properties, a bilayer structure was introduced. For example, Held et al. fabricated a bilayer hybrid dielectric consisting of a high-k hafnium oxide (HfO_x)/thin PMMA layer with a donor-acceptor polymer, poly(2,5-bis(2-octyldodecyl)–3-(5–(thieno[3,2-b]thiophen-2,5-yl)thiophen-2-yl)–6-(thiophen-2,5-yl)pyrrolo[3,4-c]pyrrole-1,4(2H,5H)-dione) (DPPT-TT) or single-walled carbon nanotubes (SWNTs) as the semiconductor [136]. PMMA layers were spin-casted and hafnium oxide layers were deposited via ALD. The resulting FETs exhibited drastically reduced operating voltages. The PMMA/HfOx hybrid dielectric exhibited low-voltage operation, well-balanced charge carrier transport, low trap densities, and excellent bias stress stability as PMMA ensures a low density of trap states at the semiconductor dielectric interface and HfO_x layers provide high capacitance (Figure 10a). Moreover, the effects of a hybrid dielectric layer for SWNT-FETs were investigated. The SWNT-FETs with only HfO_x dielectric layer exhibit strong threshold shift and hysteresis, as observed in the transfer characteristics (Figure 10b). In contrast, ambipolar transfer characteristics without hysteresis was observed in SWNT-FETs with the hybrid dielectric (Figure 10c). According to bias stress tests, SWNT-FETs with hybrid dielectric exhibit constant on-currents without any noticeable degradation over 10 h, while SWNT/HfO_x FETs suffer an on-current decay of an order of magnitude recorded in Figure 10d.

High performance low-voltage pentacene-based organic TFTs with pentacene/PMMA/Al_2O_3/ITO architecture were fabricated and their electronic characteristics were investigated [137]. In this study, a high-k metal oxide dielectric, Al_2O_3, was used due to its excellent dielectric constant (k = 7.0~9.0) and large bandgap (Eg = 8.45~9.9 eV). PMMA renders improved interfacial properties between Al_2O_3 and organic pentacene. The OFETs with only an Al_2O_3 layer exhibited a field-effect mobility of 0.65 cm^2/Vs, a threshold voltage of −0.6 V,I_{on}/I_{off} ratio of 4×10^3, and a sub-threshold swing of 0.45 V/dec, at operating voltages as low as −4 V. After being modified by PMMA, the mobility increased from 0.65 to 0.84 cm^2/Vs.

Poly(α-methylstyrene) (PαMS) was also applied on top of zirconium oxide (ZrO_2) layers to improve the quality of the interfaces between ZrO_2 and organic semiconductors [138]. In greater detail, a ZrO_2 film was synthesized on Si via a chemical solution process and annealed at temperatures between 400 and 700 °C. PαMS or HMDS layers were then spin-casted and made to undergo vacuum evaporation with pentacene. It was found that the surface modifications greatly affect the electrical performance of the ZrO_2 OTFTs. The surface energy deceased after surface modification and the calculated values are 43.9, 37.8, and 35.5 mJ/m^2 for bare-ZrO_2, HMDS-ZrO_2, and PαMS-ZrO_2, respectively, as depicted in Figure 11a–c. The PαMS modified devices exhibited a higher carrier mobility and on/off ratio than those fabricated with bare ZrO_2 and HMDS-coated ZrO_2 because the PαMS/ZrO_2 layers provide a low surface energy and thus promote the growth of large pentacene crystals. In particular, the carrier mobility of the devices with PαMS-modified ZrO_2 were observed to increase remarkably from 0.08 to 0.51 cm^2/Vs, whereas the carrier mobilities of the devices with bare ZrO_2 and HMDS-modified ZrO_2 remained at values of ~0.06 and ~0.11 cm^2/Vs, respectively, while the dielectric constant of ZrO_2 was increased from 12.17 to 19.70 (Figure 11d). Furthermore, PαMS/ZrO_2 OTFTs fabricated on flexible polyethyleneterephthalate (PET) substrate were demonstrated, as depicted in Figure 11e,f. The flexible OTFTs exhibited typical I_{DS}-V_{GS} curves of the ZrO_2-OFET, exhibiting a ~10^5 on/off-current ratio between +1 V and −5 V of V_{GS} (Figure 11g).

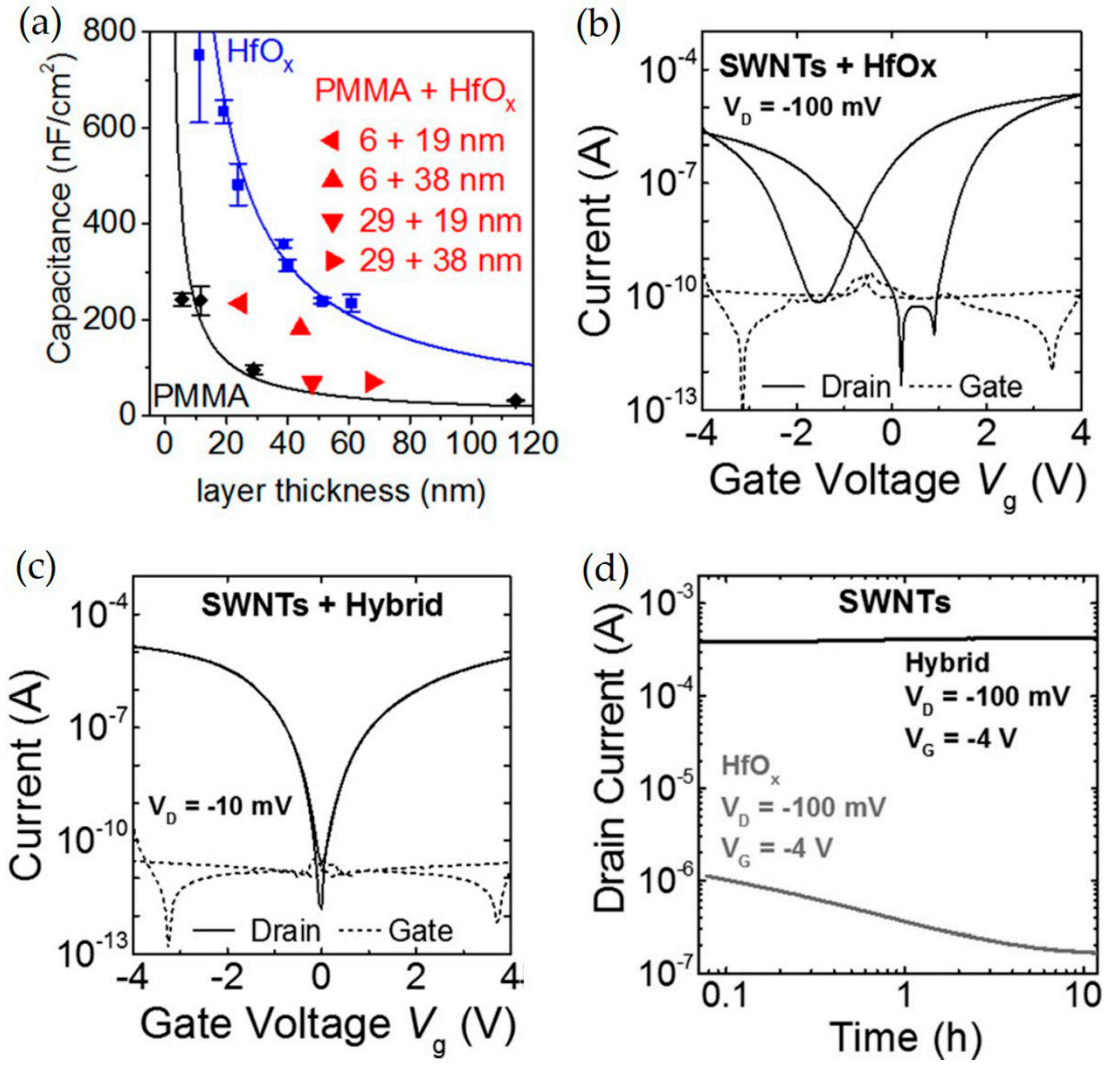

Figure 10. (**a**) Capacitance as a function of total layer thickness for hafnium oxide, PMMA, and hybrid dielectric. Transfer characteristics of network SWNT FETs with (**b**) HfO*x* and (**c**) hybrid dielectric. Channel width/length ratio and channel lengths were 125 and 40 μm, respectively. (**d**) Bias stress tests of SWNT-based transistors with different dielectrics. Reproduced with permission from [136], Copyright 2015 American Institute of Physics.

Ha et al. have reported on low-voltage OTFTs employing solution-processed hybrid bilayer gate dielectric of high-k ZrO_2 and low-k amorphous fluoropolymer, CYTOP [139]. The thin hydrophobic CYTOP layer repels aqueous molecules from an organic active layer. Therefore, such device architecture improves electronic characteristics including field effect mobility (from 0.18 to 0.28 cm^2/Vs), threshold voltage (V_{th}, from 0.4 to -0.1 V), and sub-threshold (S.S., 0.57 to 0.28 V/decade) compared to only high-k ZrO_2 devices. The reduction in defect-states at the interface suppresses photo-induced hysteresis and enhances the stability of device performance against electric bias-stress.

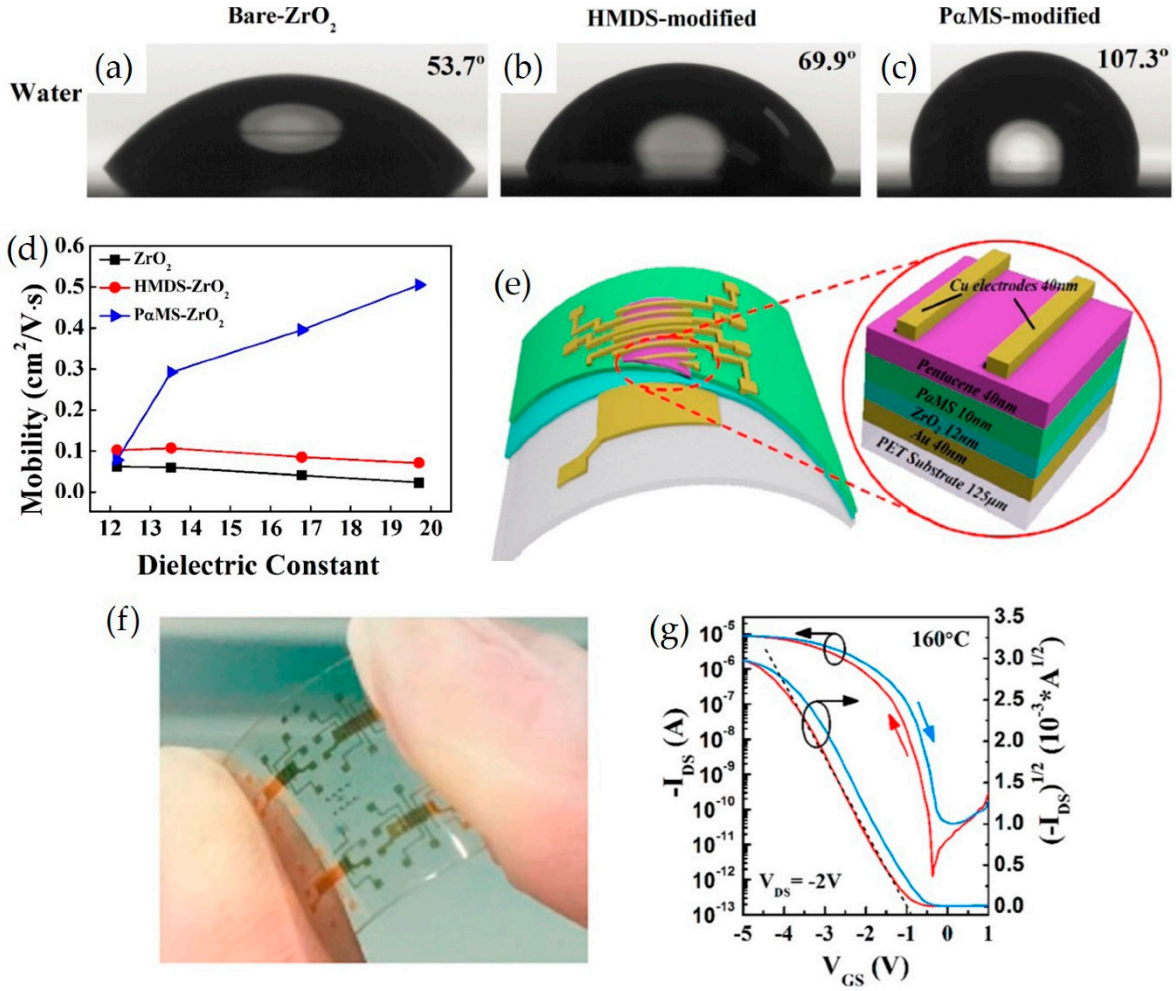

Figure 11. Water contact angles of (**a**) bare-ZrO_2 surface, (**b**) HMDS modified surface, (**c**) PαMS modified surface. (**d**) Field effect hole mobility as a function of ZrO_2 dielectric constant for OFETs with different surface modifications. The mobility was calculated with $V_G = -5$ V and capacity density under $f = 1$ kHz. (**e**) Schematic diagram of the flexible OTFT fabricated on PET substrate and (**f**) the digital photograph of the flexible OTFTs. (**g**) I_{DS}–V_{GS} transfer curves of a ZrO_2-OFET constructed on PET flexible substrate. The channel width and length of the transistor are 750 μm and 50 μm, respectively. Reproduced with permission from [138], Copyright 2016 American Chemical Society.

4. Summary and Outlook

In summary, we first give an overview of the development in polymer/metal oxide nanocomposites for applications in flexible charge transport channels and dielectrics. Recently, metal oxides (MOs) have been fabricated via vacuum-based techniques including pulsed laser deposition (PLD), atomic layer deposition (ALD), magnetron sputtering, and e-beam evaporation, for use in flexible and transparent charge transport channels. Despite their ultra-thin width, only inorganic MO films are vulnerable to repeated mechanical deformation. As a response to low mechanical durability and flexibility, hybrid polymer/MO nanocomposites have been introduced. Hybridization with soft organic materials have proven to be an effective strategy that not only offers mechanical flexibility but also enables solution-based fabrication.

Organic dielectrics have garnered substantial attention owing to their flexibility, mechanical stability, solution processability, and excellent compatibility with flexible organic substrates. However, the low k values of such materials prohibit their application in practical electronic devices. Thereby, high-k inorganic MOs have been employed as fillers. Considering that most of the flexible substrates

and semiconductors are organic materials, hybrid gate dielectrics tend to provide good compatibility with organic substrates and semiconductors.

Despite significant advances in flexible electronics by using polymers, many challenges remain to be surmounted, including poor mechanical durability, low charge-carrier mobility, and low dielectric constants. However, we believe that hybrid nanocomposites will reach their full potential in flexible electronics in the near future, as various methods to overcome their weaknesses are being continuously explored.

Author Contributions: Author Contributions: Literature search and review, J.W.J., H.S.H., D.C., J.J., and M.C.; Writing—original draft preparation, J.W.J., H.S.H., B.C.M., J.J., and M.C.; Writing—review and editing, H.S.H., B.C.M., J.J., and M.C. All authors have read and agreed to the published version of the manuscript.

Funding: This work was supported by the National Research Foundation of Korea with a grant funded by the Korean government (Ministry of Science, ICT & Future Planning, MSIP) (NRF-2017R1C1B5017856 and NRF-2017R1C1B1004605). This study was also supported by Basic Science Research Program through the National Research Foundation of Korea funded by the Ministry of Education (NRF-2019R1I1A1A01061532).

Conflicts of Interest: The authors declare no conflict of interest.

References

1. Ju, S.; Facchetti, A.; Xuan, Y.; Liu, J.; Ishikawa, F.; Ye, P.; Zhou, C.; Marks, T.J.; Janes, D.B. Fabrication of Fully Transparent Nanowire Transistors for Transparent and Flexible Electronics. *Nat. Nanotechnol.* **2007**, *2*, 378. [CrossRef]
2. Park, S.; Vosguerichian, M.; Bao, Z. A Review of Fabrication and Applications of Carbon Nanotube Film-Based Flexible Electronics. *Nanoscale* **2013**, *5*, 1727–1752. [CrossRef] [PubMed]
3. McCoul, D.; Hu, W.; Gao, M.; Mehta, V.; Pei, Q. Recent Advances in Stretchable and Transparent Electronic Materials. *Adv. Electron. Mater.* **2016**, *2*, 1500407. [CrossRef]
4. Khang, D.-Y.; Jiang, H.; Huang, Y.; Rogers, J.A. A Stretchable Form of Single-Crystal Silicon for High-Performance Electronics on Rubber Substrates. *Science* **2006**, *311*, 208–212. [CrossRef] [PubMed]
5. Kim, D.H.; Kim, Y.S.; Wu, J.; Liu, Z.; Song, J.; Kim, H.S.; Huang, Y.Y.; Hwang, K.C.; Rogers, J.A. Ultrathin Silicon Circuits with Strain-Isolation Layers and Mesh Layouts for High-Performance Electronics on Fabric, Vinyl, Leather, and Paper. *Adv. Mater.* **2009**, *21*, 3703–3707. [CrossRef]
6. Faraji, S.; Danesh, E.; Tate, D.J.; Turner, M.L.; Majewski, L.A. Cyanoethyl Cellulose-Based Nanocomposite Dielectric for Low-Voltage, Solution-Processed Organic Field-Effect Transistors (OFETs). *J. Phys. D* **2016**, *49*, 185102. [CrossRef]
7. Schroeder, R.; Majewski, L.A.; Grell, M. High-Performance Organic Transistors Using Solution-Processed Nanoparticle-Filled High-k Polymer Gate Insulators. *Adv. Mater.* **2005**, *17*, 1535–1539. [CrossRef]
8. Cai, W.; Wilson, J.; Zhang, J.; Park, S.; Majewski, L.; Song, A. Low-Voltage, Flexible InGaZnO Thin-Film Transistors Gated with Solution-Processed, Ultra-Thin Al_x O_y. *IEEE Electron Device Lett.* **2018**, *40*, 36–39.
9. Majewski, L.A.; Schroeder, R.; Grell, M. One Volt Organic Transistor. *Adv. Mater.* **2005**, *17*, 192–196. [CrossRef]
10. Cai, W.; Park, S.; Zhang, J.; Wilson, J.; Li, Y.; Xin, Q.; Majewski, L.; Song, A. One-Volt IGZO Thin-Film Transistors With Ultra-Thin, Solution-Processed Al_xO_y Gate Dielectric. *IEEE Electron Device Lett.* **2018**, *39*, 375–378. [CrossRef]
11. Cai, W.; Wilson, J.; Zhang, J.; Brownless, J.; Zhang, X.; Majewski, L.A.; Song, A. Significant Performance Enhancement of Very-Thin InGaZnO Thin-Film Transistors by a Self-Assembled Monolayer Treatment. *ACS Appl. Electron. Mater.* **2020**, *2*, 301–308. [CrossRef]
12. Lu, J.; Wong, C.P. Recent Advances in High-k Nanocomposite Materials for Embedded Capacitor Applications. *IEEE. Trans. Dielectr. Electr. Insul.* **2008**, *15*, 1322–1328.
13. Liu, J.; Buchholz, D.B.; Hennek, J.W.; Chang, R.P.; Facchetti, A.; Marks, T.J. All-Amorphous-Oxide Transparent, Flexible Thin-Film Transistors. Efficacy of Bilayer Gate Dielectrics. *J. Am. Chem. Soc.* **2010**, *132*, 11934–11942. [CrossRef] [PubMed]
14. Lee, J.-W.; Ju, B.-K.; Jang, J.; Yoon, Y.-S.; Kim, J.-K. High Mobility Organic Transistor Patterned by the Shadow-Mask with All Structure on a Plastic Substrate. *J. Mater. Sci.* **2007**, *42*, 1026–1030. [CrossRef]

15. Lee, I.-Y.; Park, H.-Y.; Park, J.-H.; Yoo, G.; Lim, M.-H.; Park, J.; Rathi, S.; Jung, W.-S.; Kim, J.; Kim, S.-W. Poly-4-vinylphenol and Poly (melamine-co-formaldehyde)-Based Graphene Passivation Method for Flexible, Wearable and Transparent Electronics. *Nanoscale* **2014**, *6*, 3830–3836. [CrossRef] [PubMed]
16. Trung, T.Q.; Tien, N.T.; Kim, D.; Jang, M.; Yoon, O.J.; Lee, N.E. A Flexible Reduced Graphene Oxide Field-Effect Transistor for Ultrasensitive Strain Sensing. *Adv. Funct. Mater.* **2014**, *24*, 117–124. [CrossRef]
17. Schattka, J.H.; Shchukin, D.G.; Jia, J.; Antonietti, M.; Caruso, R.A. Photocatalytic Activities of Porous Titania and Titania/Zirconia Structures Formed by Using a Polymer Gel Templating Technique. *Chem. Mater.* **2002**, *14*, 5103–5108. [CrossRef]
18. Kim, J.H.; Hwang, B.-U.; Kim, D.-I.; Kim, J.S.; Seol, Y.G.; Kim, T.W.; Lee, N.-E. Nanocomposites of Polyimide and Mixed Oxide Nanoparticles for High Performance Nanohybrid Gate Dielectrics in Flexible Thin Film Transistors. *Electron. Mater. Lett.* **2017**, *13*, 214–221. [CrossRef]
19. Madusanka, N.; Shivareddy, S.G.; Hiralal, P.; Eddleston, M.D.; Choi, Y.; Oliver, R.A.; Amaratunga, G.A.J. Nanocomposites of TiO_2/Cyanoethylated Cellulose with Ultra High Dielectric Constants. *Nanotechnology* **2016**, *27*, 195402. [CrossRef]
20. Beaulieu, M.R.; Baral, J.K.; Hendricks, N.R.; Tang, Y.; Briseño, A.L.; Watkins, J.J. Solution Processable High Dielectric Constant Nanocomposites Based on ZrO_2 Nanoparticles for Flexible Organic Transistors. *ACS Appl. Mater. Interfaces* **2013**, *5*, 13096–13103. [CrossRef]
21. Yang, W.; Song, K.; Jung, Y.; Jeong, S.; Moon, J. Solution-Deposited Zr-doped AlO_x Gate Dielectrics Enabling High-Performance Flexible Transparent Thin Film Transistors. *J. Mater. Chem. C* **2013**, *1*, 4275–4282. [CrossRef]
22. Min, Y.-S.; Cho, Y.J.; Hwang, C.S. Atomic Layer Deposition of Al_2O_3 Thin Films from a 1-methoxy-2-methyl-2-propoxide Complex of Aluminum and Water. *Chem. Mater.* **2005**, *17*, 626–631. [CrossRef]
23. Jeong, S.; Ha, Y.G.; Moon, J.; Facchetti, A.; Marks, T.J. Role of Gallium Doping in Dramatically Lowering Amorphous-Oxide Processing Temperatures for Solution-Derived Indium Zinc Oxide Thin-Film Transistors. *Adv. Mater.* **2010**, *22*, 1346–1350. [CrossRef] [PubMed]
24. Hennek, J.W.; Smith, J.; Yan, A.; Kim, M.-G.; Zhao, W.; Dravid, V.P.; Facchetti, A.; Marks, T.J. Oxygen "getter" Effects on Microstructure and Carrier Transport in Low Temperature Combustion-Processed a-InXZnO (X = Ga, Sc, Y, La) Transistors. *J. Am. Chem. Soc.* **2013**, *135*, 10729–10741. [CrossRef] [PubMed]
25. Banger, K.K.; Peterson, R.L.; Mori, K.; Yamashita, Y.; Leedham, T.; Sirringhaus, H. High Performance, Low Temperature Solution-Processed Barium and Strontium Doped Oxide Thin Film Transistors. *Chem. Mater.* **2014**, *26*, 1195–1203. [CrossRef] [PubMed]
26. Jo, J.W.; Kim, J.; Kim, K.T.; Kang, J.G.; Kim, M.G.; Kim, K.H.; Ko, H.; Kim, Y.H.; Park, S.K. Highly Stable and Imperceptible Electronics Utilizing Photoactivated Heterogeneous Sol-Gel Metal–Oxide Dielectrics and Semiconductors. *Adv. Mater.* **2015**, *27*, 1182–1188. [CrossRef]
27. Khanal, R.; Buchholz, D.B.; Chang, R.P.; Medvedeva, J.E. Composition-Dependent Structural and Transport Properties of Amorphous Transparent Conducting Oxides. *Phys. Rev. B* **2015**, *91*, 205203. [CrossRef]
28. Nadaud, N.; Lequeux, N.; Nanot, M.; Jove, J.; Roisnel, T. Structural Studies of Tin-Doped Indium Oxide (ITO) and $In_4Sn_3O_{12}$. *J. Solid State Chem.* **1998**, *135*, 140–148. [CrossRef]
29. Jin, S.H.; Kang, S.-K.; Cho, I.-T.; Han, S.Y.; Chung, H.U.; Lee, D.J.; Shin, J.; Baek, G.W.; Kim, T.-I.; Lee, J.-H. Water-Soluble Thin Film Transistors and Circuits Based on Amorphous Indium–Gallium–Zinc Oxide. *ACS Appl. Mater. Interfaces* **2015**, *7*, 8268–8274. [CrossRef]
30. Lim, S.H.; Kim, J.; Lee, S.-G.; Kim, Y.S. Water-Soluble Polymer Dielectric with Potential for High Performance Organic Thin-Film Transistors. *Chem. Commun.* **2010**, *46*, 3961–3963. [CrossRef]
31. Byun, H.S.; Xu, Y.-X.; Song, C.K. Fabrication of High Performance Pentacene Thin Film Transistors Using Poly (4-vinylphenol) as the Gate Insulator on Polyethyleneterephthalate Substrates. *Thin Solid Films* **2005**, *493*, 278–281. [CrossRef]
32. Kim, J.-M.; Lee, J.-W.; Kim, J.-K.; Ju, B.-K.; Kim, J.-S.; Lee, Y.-H.; Oh, M.-H. An Organic Thin-Film Transistor of High Mobility by Dielectric Surface Modification with Organic Molecule. *Appl. Phys. Lett.* **2004**, *85*, 6368–6370. [CrossRef]
33. Wei, Q.; You, E.; Hendricks, N.R.; Briseno, A.L.; Watkins, J.J. Flexible Low-Voltage Polymer Thin-Film Transistors Using Supercritical CO_2-Deposited ZrO_2 Dielectrics. *ACS Appl. Mater. Interfaces* **2012**, *4*, 2322–2324. [CrossRef] [PubMed]

34. De Angelis, F.; Cipolloni, S.; Mariucci, L.; Fortunato, G. High-Field-Effect-Mobility Pentacene Thin-Film Transistors with Polymethylmetacrylate Buffer Layer. *Appl. Phys. Lett.* **2005**, *86*, 203505. [CrossRef]
35. Kato, T.; Suzuki, T.; Amamiya, T.; Irie, T.; Komiyama, M.; Yui, H. Effects of Macromolecules on the Crystallization of $CaCO_3$ the Formation of Organic/Inorganic Composites. *Supramol. Sci.* **1998**, *5*, 411–415. [CrossRef]
36. Zukas, B.G.; Gupta, N.R. Interphase Synthesis of Zinc Oxide Nanoparticles in a Droplet Flow Reactor. *Ind. Eng. Chem. Res.* **2017**, *56*, 7184–7191. [CrossRef]
37. Ali, G.; Park, Y.J.; Kim, J.W.; Cho, S.O. A Green, General, and Ultrafast Route for the Synthesis of Diverse Metal Oxide Nanoparticles with Controllable Sizes and Enhanced Catalytic Activity. *ACS Appl. Nano Mater.* **2018**, *1*, 6112–6122. [CrossRef]
38. Cao, H.; Zhou, X.; Zheng, C.; Liu, Z. Two-Dimensional Porous Micro/Nano Metal Oxides Templated by Graphene Oxide. *ACS Appl. Mater. Interfaces* **2015**, *7*, 11984–11990. [CrossRef]
39. Niederberger, M. Nonaqueous Sol–Gel Routes to Metal Oxide Nanoparticles. *Acc. Chem. Res.* **2007**, *40*, 793–800. [CrossRef]
40. Yu, J.; Yu, X. Hydrothermal Synthesis and Photocatalytic Activity of Zinc Oxide Hollow Spheres. *Environ. Sci. Technol.* **2008**, *42*, 4902–4907. [CrossRef]
41. Ba, J.; Polleux, J.; Antonietti, M.; Niederberger, M. Non-Aqueous Synthesis of Tin Oxide Nanocrystals and Their Assembly into Ordered Porous Mesostructures. *Adv. Mater.* **2005**, *17*, 2509–2512. [CrossRef]
42. Bilecka, I.; Djerdj, I.; Niederberger, M. One-Minute Synthesis of Crystalline Binary and Ternary Metal Oxide Nanoparticles. *Chem. Commun.* **2008**, 886–888. [CrossRef] [PubMed]
43. Ding, Z.; Hu, X.; Yue, P.L.; Lu, G.Q.; Greenfield, P.F. Synthesis of Anatase TiO_2 Supported on Porous Solids by Chemical Vapor Deposition. *Catal. Today* **2001**, *68*, 173–182. [CrossRef]
44. Wang, Y.; Lei, Y.; Li, J.; Gu, L.; Yuan, H.; Xiao, D. Synthesis of 3D-Nanonet Hollow Structured Co_3O_4 for High Capacity Supercapacitor. *ACS Appl. Mater. Interfaces* **2014**, *6*, 6739–6747. [CrossRef] [PubMed]
45. Gawande, M.B.; Branco, P.S.; Parghi, K.; Shrikhande, J.J.; Pandey, R.K.; Ghumman, C.A.A.; Bundaleski, N.; Teodoro, O.M.N.D.; Jayaram, R.V. Synthesis and Characterization of Versatile MgO–ZrO_2 Mixed Metal Oxide Nanoparticles and Their Applications. *Catal. Sci. Technol.* **2011**, *1*, 1653–1664. [CrossRef]
46. Sharma, R.K.; Ghose, R. Synthesis of Nanocrystalline CuO–ZnO Mixed Metal Oxide Powder by a Homogeneous Precipitation Method. *Ceram. Int.* **2014**, *40*, 10919–10926. [CrossRef]
47. Li, J.; Liu, X.; Cui, J.; Sun, J. Hydrothermal Synthesis of Self-Assembled Hierarchical Tungsten Oxides Hollow Spheres and Their Gas Sensing Properties. *ACS Appl. Mater. Interfaces* **2015**, *7*, 10108–10114. [CrossRef]
48. Van Tong, P.; Hoa, N.D.; Van Duy, N.; Le, D.T.T.; Van Hieu, N. Enhancement of Gas-Sensing Characteristics of Hydrothermally Synthesized WO_3 Nanorods by Surface Decoration with Pd Nanoparticles. *Sens. Actuators B Chem.* **2016**, *223*, 453–460. [CrossRef]
49. Yeo, J.; Hong, S.; Kim, G.; Lee, H.; Suh, Y.D.; Park, I.; Grigoropoulos, C.P.; Ko, S.H. Laser-Induced Hydrothermal Growth of Heterogeneous Metal-Oxide Nanowire on Flexible Substrate by Laser Absorption Layer Design. *ACS Nano* **2015**, *9*, 6059–6068. [CrossRef]
50. Wang, J.; Yang, P.; Wei, X. High-Performance, Room-Temperature, and No-Humidity-Impact Ammonia Sensor Based on Heterogeneous Nickel Oxide and Zinc Oxide Nanocrystals. *ACS Appl. Mater. Interfaces* **2015**, *7*, 3816–3824. [CrossRef]
51. Lu, B.; Bai, J.; Bo, X.; Zhu, L.; Guo, L. A Simple Hydrothermal Synthesis of Nickel Hydroxide–Ordered Mesoporous Carbons Nanocomposites and Its Electrocatalytic Application. *Electrochim. Acta* **2010**, *55*, 8724–8730. [CrossRef]
52. Liu, Q.; Qin, M.C.; Ke, W.J.; Zheng, X.L.; Chen, Z.; Qin, P.L.; Xiong, L.B.; Lei, H.W.; Wan, J.W.; Wen, J. Enhanced Stability of Perovskite Solar Cells with Low-Temperature Hydrothermally Grown SnO_2 Electron Transport Layers. *Adv. Funct. Mater.* **2016**, *26*, 6069–6075. [CrossRef]
53. Ji, H.; Miao, X.; Wang, L.; Qian, B.; Yang, G. Microwave-Assisted Hydrothermal Synthesis of Sphere-like C/CuO and CuO Nanocrystals and Improved Performance as Anode Materials for Lithium-Ion Batteries. *Powder Technol.* **2013**, *241*, 43–48. [CrossRef]
54. Yayapao, O.; Thongtem, T.; Phuruangrat, A.; Thongtem, S. CTAB-Assisted Hydrothermal Synthesis of Tungsten Oxide Microflowers. *J. Alloys Compd.* **2011**, *509*, 2294–2299. [CrossRef]

55. Zhao, R.; Wang, L.; Chai, Z.-F.; Shi, W.-Q. Synthesis of ThO_2 Nanostructures through a Hydrothermal Approach: Influence of Hexamethylenetetramine (HMTA) and Sodium Dodecyl Sulfate (SDS). *RSC Adv.* **2014**, *4*, 52209–52214. [CrossRef]
56. Xiao, W.; Wang, Z.; Guo, H.; Zhang, Y.; Zhang, Q.; Gan, L. A Facile PVP-Assisted Hydrothermal Fabrication of Fe_2O_3/Graphene Composite as High Performance Anode Material for Lithium Ion Batteries. *J. Alloys Compd.* **2013**, *560*, 208–214. [CrossRef]
57. Vishwas, M.; Narasimha Rao, K.; Arjuna Gowda, K.V.; Chakradhar, R.P.S. Influence of Sn Doping on Structural, Optical and Electrical Properties of ZnO Thin Films Prepared by Cost Effective Sol–Gel Process. *Spectrochim. Acta A* **2012**, *95*, 423–426. [CrossRef]
58. Li, X.; Liu, P.; Mao, Y.; Xing, M.; Zhang, J. Preparation of Homogeneous Nitrogen-Doped Mesoporous TiO_2 Spheres with Enhanced Visible-Light Photocatalysis. *Appl. Catal. B Environ.* **2015**, *164*, 352–359. [CrossRef]
59. Soo, M.T.; Prastomo, N.; Matsuda, A.; Kawamura, G.; Muto, H.; Noor, A.F.M.; Lockman, Z.; Cheong, K.Y. Elaboration and Characterization of Sol–Gel Derived ZrO_2 Thin Films Treated with Hot Water. *Appl. Surf. Sci.* **2012**, *258*, 5250–5258. [CrossRef]
60. Niederberger, M.; Garnweitner, G.; Buha, J.; Polleux, J.; Ba, J.; Pinna, N. Nonaqueous Synthesis of Metal Oxide Nanoparticles:Review and Indium Oxide as Case Study for the Dependence of Particle Morphology on Precursors and Solvents. *J. Sol-Gel Sci. Technol.* **2006**, *40*, 259–266. [CrossRef]
61. Athar, T.; Hakeem, A.; Ahmed, W. Synthesis of MgO Nanopowder via Non Aqueous Sol–gel Method. *Adv. Sci. Lett.* **2012**, *7*, 27–29. [CrossRef]
62. Masthoff, I.C.; Kraken, M.; Menzel, D.; Litterst, F.J.; Garnweitner, G. Study of the Growth of Hydrophilic Iron Oxide Nanoparticles Obtained via the Non-Aqueous Sol–Gel Method. *J. Sol-Gel Sci. Technol.* **2016**, *77*, 553–564. [CrossRef]
63. Singh, I.; Kumar, R.; Birajdar, B.I. Zirconium Doped TiO_2 Nano-Powder via Halide Free Non-Aqueous Solvent Controlled Sol–gel Route. *J. Environ. Chem. Eng.* **2017**, *5*, 2955–2963. [CrossRef]
64. Niederberger, M.; Bartl, M.H.; Stucky, G.D. Benzyl Alcohol and Transition Metal Chlorides as a Versatile Reaction System for the Nonaqueous and Low-Temperature Synthesis of Crystalline Nano-Objects with Controlled Dimensionality. *J. Am. Chem. Soc.* **2002**, *124*, 13642–13643. [CrossRef] [PubMed]
65. Mirzaei, A.; Neri, G. Microwave-Assisted Synthesis of Metal Oxide Nanostructures for Gas Sensing Application: A Review. *Sens. Actuators B Chem.* **2016**, *237*, 749–775. [CrossRef]
66. Xi, G.; He, Y.; Zhang, Q.; Xiao, H.; Wang, X.; Wang, C. Synthesis of Crystalline Microporous SnO_2 via a Surfactant-Assisted Microwave Heating Method: A General and Rapid Method for the Synthesis of Metal Oxide Nanostructures. *J. Phys. Chem. C* **2008**, *112*, 11645–11649. [CrossRef]
67. Vijayakumar, S.; Nagamuthu, S.; Muralidharan, G. Supercapacitor Studies on NiO Nanoflakes Synthesized Through a Microwave Route. *ACS Appl. Mater. Interfaces* **2013**, *5*, 2188–2196. [CrossRef]
68. Mondal, A.K.; Su, D.; Chen, S.; Kretschmer, K.; Xie, X.; Ahn, H.-J.; Wang, G. A Microwave Synthesis of Mesoporous $NiCo_2O_4$ Nanosheets as Electrode Materials for Lithium-Ion Batteries and Supercapacitors. *ChemPhysChem* **2015**, *16*, 169–175. [CrossRef]
69. Ede, S.R.; Anantharaj, S.; Subramanian, B.; Rathishkumar, A.; Kundu, S. Microwave-Assisted Template-Free Synthesis of $Ni_3(BO_3)_2$(NOB) Hierarchical Nanoflowers for Electrocatalytic Oxygen Evolution. *Energy Fuels* **2018**, *32*, 6224–6233. [CrossRef]
70. Bilecka, I.; Niederberger, M. Microwave Chemistry for Inorganic Nanomaterials Synthesis. *Nanoscale* **2010**, *2*, 1358–1374. [CrossRef]
71. Nomura, K.; Ohta, H.; Takagi, A.; Kamiya, T.; Hirano, M.; Hosono, H. Room-Temperature Fabrication of Transparent Flexible Thin-Film Transistors Using Amorphous Oxide Semiconductors. *Nature* **2004**, *432*, 488–492. [CrossRef] [PubMed]
72. Buchholz, D.B.; Ma, Q.; Alducin, D.; Ponce, A.; Jose-Yacaman, M.; Khanal, R.; Medvedeva, J.E.; Chang, R.P.H. The Structure and Properties of Amorphous Indium Oxide. *Chem. Mater.* **2014**, *26*, 5401–5411. [CrossRef] [PubMed]
73. Thomas, S.R.; Pattanasattayavong, P.; Anthopoulos, T.D. Solution-Processable Metal Oxide Semiconductors for Thin-Film Transistor Applications. *Chem. Soc. Rev.* **2013**, *42*, 6910–6923. [CrossRef] [PubMed]
74. Xu, H.; Luo, D.; Li, M.; Xu, M.; Zou, J.; Tao, H.; Lan, L.; Wang, L.; Peng, J.; Cao, Y. A Flexible AMOLED Display on the PEN Substrate Driven by Oxide Thin-Film Transistors Using Anodized Aluminium Oxide as Dielectric. *J. Mater. Chem. C* **2014**, *2*, 1255–1259. [CrossRef]

75. Cairns, D.R.; Witte, R.P.; Sparacin, D.K.; Sachsman, S.M.; Paine, D.C.; Crawford, G.P.; Newton, R.R. Strain-Dependent Electrical Resistance of Tin-Doped Indium Oxide on Polymer Substrates. *Appl. Phys. Lett.* **2000**, *76*, 1425–1427. [CrossRef]
76. Peng, C.; Jia, Z.; Bianculli, D.; Li, T.; Lou, J. In Situ Electro-Mechanical Experiments and Mechanics Modeling of Tensile Cracking in Indium Tin Oxide Thin Films on Polyimide Substrates. *J. Appl. Phys.* **2011**, *109*, 103530. [CrossRef]
77. Xing, G.Z.; Yi, J.B.; Yan, F.; Wu, T.; Li, S. Positive Magnetoresistance in Ferromagnetic Nd-Doped In_2O_3 Thin Films Grown by Pulse Laser Deposition. *Appl. Phys. Lett.* **2014**, *104*, 202411. [CrossRef]
78. Imai, H.; Tominaga, A.; Hirashima, H.; Toki, M.; Asakuma, N. Ultraviolet-Reduced Reduction and Crystallization of Indium Oxide Films. *J. Appl. Phys.* **1999**, *85*, 203–207. [CrossRef]
79. Kim, J.Y.; Lee, K.; Coates, N.E.; Moses, D.; Nguyen, T.-Q.; Dante, M.; Heeger, A.J. Efficient Tandem Polymer Solar Cells Fabricated by All-Solution Processing. *Science* **2007**, *317*, 222–225. [CrossRef]
80. Ma, W.; Yang, C.; Gong, X.; Lee, K.; Heeger, A.J. Thermally Stable, Efficient Polymer Solar Cells with Nanoscale Control of the Interpenetrating Network Morphology. *Adv. Funct. Mater.* **2005**, *15*, 1617–1622. [CrossRef]
81. Le, T.-H.; Kim, Y.; Yoon, H. Electrical and Electrochemical Properties of Conducting Polymers. *Polymers* **2017**, *9*, 150. [CrossRef] [PubMed]
82. Kong, H.J.; Kim, S.; Le, T.-H.; Kim, Y.; Park, G.; Park, C.S.; Kwon, O.S.; Yoon, H. Nanostructured Mesophase Electrode Materials: Modulating Charge-Storage Behavior by Thermal Treatment. *Nanoscale* **2017**, *9*, 17450–17458. [CrossRef] [PubMed]
83. Beek, W.J.; Slooff, L.H.; Wienk, M.M.; Kroon, J.M.; Janssen, R.A. Hybrid Solar Cells Using a Zinc Oxide Precursor and a Conjugated Polymer. *Adv. Funct. Mater.* **2005**, *15*, 1703–1707. [CrossRef]
84. Chen, C.-T.; Hsu, F.-C.; Kuan, S.-W.; Chen, Y.-F. The Effect of C60 on the ZnO-Nanorod Surface in Organic–Inorganic Hybrid Photovoltaics. *Sol. Energy Mater. Sol. Cells* **2011**, *95*, 740–744. [CrossRef]
85. Benabid, F.; Kharchi, N.; Zouai, F.; Mourad, A.-H.I.; Benachour, D. Impact of Co-Mixing Technique and Surface Modification of ZnO Nanoparticles Using Stearic Acid on Their Dispersion into HDPE to Produce HDPE/ZnO Nanocomposites. *Polym. Polym. Compos.* **2019**, *27*, 389–399. [CrossRef]
86. Vivekchand, S.; Kam, K.C.; Gundiah, G.; Govindaraj, A.; Cheetham, A.; Rao, C. Electrical Properties of Inorganic Nanowire–Polymer Composites. *J. Mater. Chem.* **2005**, *15*, 4922–4927. [CrossRef]
87. Shim, M.; Javey, A.; Shi Kam, N.W.; Dai, H. Polymer Functionalization for Air-Stable n-Type Carbon Nanotube Field-Effect Transistors. *J. Am. Chem. Soc.* **2001**, *123*, 11512–11513. [CrossRef]
88. Du, Y.; Liu, H.; Neal, A.T.; Si, M.; Ye, P.D. Molecular Doping of Multilayer MoS_2 Field-Effect Transistors: Reduction in Sheet and Contact Resistances. *IEEE Electron Device Lett.* **2013**, *34*, 1328–1330. [CrossRef]
89. Sun, B.; Hong, W.; Thibau, E.S.; Aziz, H.; Lu, Z.-H.; Li, Y. Polyethylenimine (PEI) As an Effective Dopant To Conveniently Convert Ambipolar and p-Type Polymers into Unipolar n-Type Polymers. *ACS Appl. Mater. Interfaces* **2015**, *7*, 18662–18671. [CrossRef]
90. Fabiano, S.; Braun, S.; Liu, X.; Weverberghs, E.; Gerbaux, P.; Fahlman, M.; Berggren, M.; Crispin, X. Poly(ethylene imine) Impurities Induce n-doping Reaction in Organic (Semi)Conductors. *Adv. Mater.* **2014**, *26*, 6000–6006. [CrossRef]
91. Yu, X.; Zeng, L.; Zhou, N.; Guo, P.; Shi, F.; Buchholz, D.B.; Ma, Q.; Yu, J.; Dravid, V.P.; Chang, R.P.H.; et al. Ultra-Flexible, "Invisible" Thin-Film Transistors Enabled by Amorphous Metal Oxide/Polymer Channel Layer Blends. *Adv. Mater.* **2015**, *27*, 2390–2399. [CrossRef]
92. Jeong, E.G.; Kwon, J.H.; Kang, K.S.; Jeong, S.Y.; Choi, K.C. A Review of Highly Reliable Flexible Encapsulation Technologies towards Rollable and Foldable OLEDs. *J. Inf. Disp.* **2019**, 19–32. [CrossRef]
93. Huang, W.; Zeng, L.; Yu, X.; Guo, P.; Wang, B.; Ma, Q.; Chang, R.P.H.; Yu, J.; Bedzyk, M.J.; Marks, T.J.; et al. Metal Oxide Transistors via Polyethylenimine Doping of the Channel Layer: Interplay of Doping, Microstructure, and Charge Transport. *Adv. Funct. Mater.* **2016**, *26*, 6179–6187. [CrossRef]
94. Huang, W.; Guo, P.; Zeng, L.; Li, R.; Wang, B.; Wang, G.; Zhang, X.; Chang, R.P.H.; Yu, J.; Bedzyk, M.J.; et al. Metal Composition and Polyethylenimine Doping Capacity Effects on Semiconducting Metal Oxide—Polymer Blend Charge Transport. *J. Am. Chem. Soc.* **2018**, *140*, 5457–5473. [CrossRef] [PubMed]
95. Na, J.W.; Kim, H.J.; Hong, S.; Kim, H.J. Plasma Polymerization Enabled Polymer/Metal–Oxide Hybrid Semiconductors for Wearable Electronics. *ACS Appl. Mater. Interfaces* **2018**, *10*, 37207–37215. [CrossRef] [PubMed]

96. Sun, D.; Chen, C.; Zhang, J.; Wu, X.; Chen, H.; Guo, T. High Performance Inkjet-Printed Metal Oxide Thin Film Transistors via Addition of Insulating Polymer with Proper Molecular Weight. *Appl. Phys. Lett.* **2018**, *112*, 012102. [CrossRef]
97. Ha, Y.-G.; Everaerts, K.; Hersam, M.C.; Marks, T.J. Hybrid Gate Dielectric Materials for Unconventional Electronic Circuitry. *Acc. Chem. Res.* **2014**, *47*, 1019–1028. [CrossRef]
98. Wang, G.; Persson, N.; Chu, P.-H.; Kleinhenz, N.; Fu, B.; Chang, M.; Deb, N.; Mao, Y.; Wang, H.; Grover, M.A.; et al. Microfluidic Crystal Engineering of π-Conjugated Polymers. *ACS Nano* **2015**, *9*, 8220–8230. [CrossRef]
99. Yeon Kwon, J.; Kyeong Jeong, J. Recent Progress in High Performance and Reliable N-type Transition Metal Oxide-Based Thin Film Transistors. *Semicond. Sci. Technol.* **2015**, *30*, 024002. [CrossRef]
100. Wager, J.F.; Yeh, B.; Hoffman, R.L.; Keszler, D.A. An Amorphous Oxide Semiconductor Thin-Film Transistor Route to Oxide Electronics. *Curr. Opin. Solid State Mater. Sci.* **2014**, *18*, 53–61. [CrossRef]
101. Navan, R.R.; Prashanthi, K.; Shojaei Baghini, M.; Ramgopal Rao, V. Solution Processed Photopatternable High-k Nanocomposite Gate Dielectric for Low Voltage Organic Field Effect Transistors. *Microelectron. Eng.* **2012**, *96*, 92–95. [CrossRef]
102. Lim, S.; Lee, K.H.; Kim, H.; Kim, S.H. Optimization of Nanocomposite Gate Insulators for Organic Thin Film Transistors. *Org. Electron.* **2015**, *17*, 144–150. [CrossRef]
103. Hou, X.; Ng, S.C.; Zhang, J.; Chang, J.S. Polymer Nanocomposite Dielectric Based on P(VDF-TrFE)/PMMA/$BaTiO_3$ for TIPs-Pentacene OFETs. *Org. Electron.* **2015**, *17*, 247–252. [CrossRef]
104. Rasul, A.; Zhang, J.; Gamota, D.; Takoudis, C. High K Nanocomposite Dielectric for Printed Organic Electronics Applications. *Microelectron. Eng.* **2012**, *93*, 95–99. [CrossRef]
105. Pecunia, V.; Banger, K.; Sirringhaus, H. High-Performance Solution-Processed Amorphous-Oxide-Semiconductor TFTs with Organic Polymeric Gate Dielectrics. *Adv. Electron. Mater.* **2015**, *1*, 1400024. [CrossRef]
106. Sirringhaus, H. 25th Anniversary Article: Organic Field-Effect Transistors: The Path Beyond Amorphous Silicon. *Adv. Mater.* **2014**, *26*, 1319–1335. [CrossRef]
107. Zhang, L.; Wang, H.; Zhao, Y.; Guo, Y.; Hu, W.; Yu, G.; Liu, Y. Substrate-Free Ultra-Flexible Organic Field-Effect Transistors and Five-Stage Ring Oscillators. *Adv. Mater.* **2013**, *25*, 5455–5460. [CrossRef]
108. Khim, D.; Xu, Y.; Baeg, K.-J.; Kang, M.; Park, W.-T.; Lee, S.-H.; Kim, I.-B.; Kim, J.; Kim, D.-Y.; Liu, C.; et al. Large Enhancement of Carrier Transport in Solution-Processed Field-Effect Transistors by Fluorinated Dielectric Engineering. *Adv. Mater.* **2016**, *28*, 518–526. [CrossRef]
109. Li, J.; Liu, D.; Miao, Q.; Yan, F. The Application of a high-k Polymer in Flexible Low-Voltage Organic Thin-Film Transistors. *J. Mater. Chem.* **2012**, *22*, 15998–16004. [CrossRef]
110. Fukuda, K.; Sekine, T.; Shiwaku, R.; Morimoto, T.; Kumaki, D.; Tokito, S. Free-Standing Organic Transistors and Circuits with Sub-Micron Thicknesses. *Sci. Rep.* **2016**, *6*, 27450. [CrossRef]
111. Yu, X.; Smith, J.; Zhou, N.; Zeng, L.; Guo, P.; Xia, Y.; Alvarez, A.; Aghion, S.; Lin, H.; Yu, J.; et al. Spray-Combustion Synthesis: Efficient Solution Route to High-Performance Oxide Transistors. *Proc. Natl. Acad. Sci. USA* **2015**, *112*, 3217–3222. [CrossRef] [PubMed]
112. Chen, H.; Cao, Y.; Zhang, J.; Zhou, C. Large-Scale Complementary Macroelectronics Using Hybrid Integration of Carbon Nanotubes and IGZO Thin-Film Transistors. *Nat. Commun.* **2014**, *5*, 4097. [CrossRef] [PubMed]
113. Rasul, A.; Zhang, J.; Gamota, D.; Singh, M.; Takoudis, C. Flexible High Capacitance Nanocomposite Gate Insulator for Printed Oorganic Field-Effect Transistors. *Thin Solid Films* **2010**, *518*, 7024–7028. [CrossRef]
114. Yang, F.-Y.; Hsu, M.-Y.; Hwang, G.-W.; Chang, K.-J. High-Performance Poly(3-hexylthiophene) Top-Gate Transistors Incorporating TiO_2 Nanocomposite Dielectrics. *Org. Electron.* **2010**, *11*, 81–88. [CrossRef]
115. Park, J.; Lee, J.W.; Kim, D.W.; Park, B.J.; Choi, H.J.; Choi, J.S. Pentacene Thin-Film Transistor with Poly(methyl methacrylate-co-methacrylic acid)/TiO_2 Nanocomposite Gate Insulator. *Thin Solid Films* **2009**, *518*, 588–590. [CrossRef]
116. Lee, W.-H.; Wang, C.C. Effect of Nanocomposite Gate Dielectric Rroughness on Pentacene Field-Effect Transistor. *J. Vac. Sci. Technol. B* **2009**, *27*, 1116–1121. [CrossRef]
117. Lee, W.-H.; Wang, C.C.; Ho, J.C. Improved Performance of Pentacene Field-Effect Transistors Using a Nanocomposite Gate Dielectric. *J. Vac. Sci. Technol. B* **2009**, *27*, 601–605. [CrossRef]
118. Noh, H.Y.; Seol, Y.G.; Kim, S.I.; Lee, N.E. Mechanically Flexible Low-Leakage Nanocomposite Gate Dielectrics for Flexible Organic Thin-Film Transistors. *Electrochem. Solid State Lett.* **2008**, *11*, H218–H221. [CrossRef]

119. Kim, P.; Zhang, X.-H.; Domercq, B.; Jones, S.C.; Hotchkiss, P.J.; Marder, S.R.; Kippelen, B.; Perry, J.W. Solution-Processible High-Permittivity Nanocomposite Gate Insulators for Organic Field-Effect Transistors. *Appl. Phys. Lett.* **2008**, *93*, 013302. [CrossRef]
120. Mohammadian, N.; Faraji, S.; Sagar, S.; Das, B.C.; Turner, M.L.; Majewski, L.A. One-Volt, Solution-Processed Organic Transistors with Self-Assembled Monolayer-Ta_2O_5 Gate Dielectrics. *Materials* **2019**, *12*, 2563. [CrossRef]
121. Jung, Y.; Jun, T.; Kim, A.; Song, K.; Yeo, T.H.; Moon, J. Direct Photopatternable Organic–Inorganic Hybrid Gate Dielectric for Solution-Processed Flexible ZnO Thin Film Transistors. *J. Mater. Chem.* **2011**, *21*, 11879–11885. [CrossRef]
122. Ha, Y.-G.; Jeong, S.; Wu, J.; Kim, M.-G.; Dravid, V.P.; Facchetti, A.; Marks, T.J. Flexible Low-Voltage Organic Thin-Film Transistors Enabled by Low-Temperature, Ambient Solution-Processable Inorganic/Organic Hybrid Gate Dielectrics. *J. Am. Chem. Soc.* **2010**, *132*, 17426–17434. [CrossRef]
123. Morales-Acosta, M.D.; Quevedo-Lopez, M.A.; Gnade, B.E.; Ramírez-Bon, R.M. PMMA-SiO_2 Organic–Inorganic Hybrid Films: Determination of Dielectric Characteristics. *J. Sol-Gel Sci. Technol.* **2011**, *58*, 218–224. [CrossRef]
124. Morales-Acosta, M.D.; Quevedo-López, M.A.; Ramírez-Bon, R. PMMA–SiO_2 Hybrid Films as Gate Dielectric for ZnO Based Thin-Film Transistors. *Mater. Chem. Phys.* **2014**, *146*, 380–388. [CrossRef]
125. Morales-Acosta, M.D.; Alvarado-Beltrán, C.G.; Quevedo-López, M.A.; Gnade, B.E.; Mendoza-Galván, A.; Ramírez-Bon, R. Adjustable Structural, Optical and Dielectric Characteristics in Sol–Gel PMMA–SiO_2 Hybrid Films. *J. Non-Cryst. Solids* **2013**, *362*, 124–135. [CrossRef]
126. Alvarado-Beltrán, C.G.; Almaral-Sánchez, J.L.; Ramírez-Bon, R. Synthesis and Properties of PMMA-ZrO_2 Organic–Inorganic Hybrid Films. *J. Appl. Polym. Sci.* **2015**, *132*. [CrossRef]
127. Lee, W.-J.; Park, W.-T.; Park, S.; Sung, S.; Noh, Y.-Y.; Yoon, M.-H. Large-Scale Precise Printing of Ultrathin Sol–Gel Oxide Dielectrics for Directly Patterned Solution-Processed Metal Oxide Transistor Arrays. *Adv. Mater.* **2015**, *27*, 5043–5048. [CrossRef]
128. Lin, Y.-H.; Thomas, S.R.; Faber, H.; Li, R.; McLachlan, M.A.; Patsalas, P.A.; Anthopoulos, T.D. Al-Doped ZnO Transistors Processed from Solution at 120 °C. *Adv. Electron. Mater.* **2016**, *2*, 1600070. [CrossRef]
129. Alvarado-Beltrán, C.G.; Almaral-Sánchez, J.L.; Mejia, I.; Quevedo-López, M.A.; Ramirez-Bon, R. Sol–Gel PMMA–ZrO_2 Hybrid Layers as Gate Dielectric for Low-Temperature ZnO-Based Thin-Film Transistors. *ACS Omega* **2017**, *2*, 6968–6974. [CrossRef] [PubMed]
130. Shen, Q.; Ogomi, Y.; Chang, J.; Tsukamoto, S.; Kukihara, K.; Oshima, T.; Osada, N.; Yoshino, K.; Katayama, K.; Toyoda, T.; et al. Charge Transfer and Recombination at the Metal Oxide/$CH_3NH_3PbCl_2$/Spiro-OMeTAD Interfaces: Uncovering the Detailed Mechanism Behind High Efficiency Solar Cells. *Phys. Chem. Chem. Phys.* **2014**, *16*, 19984–19992. [CrossRef] [PubMed]
131. Kwon, J.-H.; Zhang, X.; Piao, S.H.; Choi, H.J.; Bae, J.-H.; Park, J. Stability Study of Flexible 6,13-Bis(triisopropylsilylethynyl)pentacene Thin-Film Transistors with a Cross-Linked Poly(4-vinylphenol)/Yttrium Oxide Nanocomposite Gate Insulator. *Polymers* **2016**, *8*, 88. [CrossRef] [PubMed]
132. Kim, J.; Lim, S.H.; Kim, Y.S. Solution-Based TiO_2−Polymer Composite Dielectric for Low Operating Voltage OTFTs. *J. Am. Chem. Soc.* **2010**, *132*, 14721–14723. [CrossRef] [PubMed]
133. Bang, S.; Lee, S.; Jeon, S.; Kwon, S.; Jeong, W.; Kim, H.; Shin, I.; Chang, H.J.; Park, H.-h.; Jeon, H. Al_2O_3 Buffer in a ZnO Thin Film Transistor with Poly-4-vinylphenol Dielectric. *Semicond. Sci. Technol.* **2008**, *24*, 025008. [CrossRef]
134. Kim, M.J.; Pak, K.; Hwang, W.S.; Im, S.G.; Cho, B.J. Novel Vapor-Phase Synthesis of Flexible, Homogeneous Organic–Inorganic Hybrid Gate Dielectric with sub 5 nm Equivalent Oxide Thickness. *ACS Appl. Mater. Interfaces* **2018**, *10*, 37326–37334. [CrossRef]
135. Son, B.-G.; Je, S.Y.; Kim, H.J.; Jeong, J.K. Modification of a Polymer Gate Insulator by Zirconium Oxide Doping for Low Temperature, High Performance Indium Zinc Oxide Transistors. *RSC Adv.* **2014**, *4*, 45742–45748. [CrossRef]
136. Held, M.; Schießl, S.P.; Miehler, D.; Gannott, F.; Zaumseil, J. Polymer/Metal Oxide Hybrid Dielectrics for Low Voltage Field-Effect Transistors with Solution-Processed, High-Mobility Semiconductors. *Appl. Phys. Lett.* **2015**, *107*, 083301. [CrossRef]

137. Ye, X.; Lin, H.; Yu, X.; Han, S.; Shang, M.; Zhang, L.; Jiang, Q.; Zhong, J. High Performance Low-Voltage Organic Field-Effect Transistors Enabled by Solution Processed Alumina and Polymer Bilayer Dielectrics. *Synth. Met.* **2015**, *209*, 337–342. [CrossRef]
138. He, W.; Xu, W.; Peng, Q.; Liu, C.; Zhou, G.; Wu, S.; Zeng, M.; Zhang, Z.; Gao, J.; Gao, X.; et al. Surface Modification on Solution Processable ZrO_2 High-k Dielectrics for Low Voltage Operations of Organic Thin Film Transistors. *J. Phys. Chem. C* **2016**, *120*, 9949–9957. [CrossRef]
139. Ha, T.-J. Low-Voltage and Hysteresis-Free Organic Thin-Film Transistors Employing Solution-Processed Hybrid Bilayer Gate Dielectrics. *Appl. Phys. Lett.* **2014**, *105*, 043305. [CrossRef]